Optimal control in a magnetization-prepared rapid acquisition gradient-echo sequence

Benoît Vernier, Eric van Reeth van Reeth, Frank Pilleul, Marc Lapert, Olivier Beuf, Helene Ratiney

Received: 22 July 2022 | Revised: 27 July 2023 | Accepted: 9 August 2023

DOI: 10.1002/nbm.5041

RESEARCH ARTICLE

NMR IN BIOMEDICINE WILEY

Optimal control in a magnetization-prepared rapid acquisition gradient-echo sequence

Benoît Vernier[1,2] | Eric Van Reeth[1,3] | Frank Pilleul[1,4] | Marc Lapert[2] | Oliver Beuf[1] | Hélène Ratiney[1]

[1]Univ Lyon, INSA Lyon, Inserm, UCBL, CNRS, CREATIS, UMR5220, U1294, Villeurbanne, France

[2]SIEMENS Healthcare SAS, Saint-Denis, France

[3]CPE, Lyon, France

[4]Department of Radiology, Centre de lutte contre le cancer Léon Bérard (CLB), Lyon, France

Correspondence
Eric Van Reeth, Univ Lyon, INSA Lyon, Inserm, UCBL, CNRS, CREATIS, UMR5220, U1294, Villeurbanne, France.
Email: eric.van-reeth@creatis.insa-lyon.fr

Funding information
CIFRE Siemens Healthcare SAS, Grant/Award Number: 2019/0276

Abstract

This article proposes a numerical framework to determine the optimal magnetization preparation in a three-dimensional magnetization-prepared rapid gradient-echo (MP-RAGE) sequence to obtain the best achievable contrast between target tissues based on differences in their relaxation times. The benefit lies in the adaptation of the algorithm of optimal control, GRAdient Ascent Pulse Engineering (GRAPE), to the optimization of magnetization preparation in a cyclic sequence without full recovery between each cycle. This numerical approach optimizes magnetization preparation of an arbitrary number of radio frequency pulses to enhance contrast, taking into account the establishment of a steady state in the longitudinal component of the magnetization. The optimal control preparation offers an optimized mixed T_1/T_2 contrast in this traditional T_1-weighted sequence. To show the versatility of the proposed method, numerical and in vitro results are described. Examples of contrasts acquired on brain regions of a healthy volunteer are presented for potential applications at 3 T.

KEYWORDS
Bloch equations; brain, contrast; MP-RAGE; optimal control; preparation pulses

1 | INTRODUCTION

Since the early work of Mugler and Brookeman,[1] magnetization-prepared rapid gradient-echo (MP-RAGE) has been the most common sequence for T_1-weighted magnetic resonance imaging (MRI) of the brain. This sequence allows high spatial resolution and high contrast images with durations adapted to a clinical context. An MP-RAGE sequence is divided into cycles (or segments). Each cycle contains three periods: (1) a time devoted to partial magnetization recovery; (2) a magnetization preparation period for contrast control; and (3) several data acquisitions with a short time of repetition and low flip angle using a spoiled gradient echo scheme. The repetition of these cycles leads to the establishment of a longitudinal steady state that requires disrupting transverse coherence prior to each excitation of the acquisition. In practice, disrupting transverse coherence is achieved by incrementing the RF pulse phase and using gradient spoiler.[2]

Abbreviations: CNR, contrast-to-noise ratio; CSF, cerebrospinal fluid; DBS, deep brain stimulation; FGATIR, Fast Gray matter Acquisition T_1 Inversion Recovery; FLASH, Fast Low Angle SHot magnetic resonance imaging; GM, gray matter; GRAPE, GRAdient Ascent Pulse Engineering; L-BFGS, Limited-Memory Broyden–Fletcher–Goldfarb–Shanno algorithm; MP-RAGE, magnetization-prepared rapid gradient-echo; Np.-OC-Prep, N-pulse optimal control preparation; OC, optimal control; SNR, signal-to-noise ratio; SQP, sequential quadratic programming; T_s, time of a segment; WM, white matter.

Different preparations have been described in the literature: inversion-recovery,[3] T_2Prep,[4] and IR-T_2Prep.[5] In clinical routine, the MP-RAGE sequence is used with an inversion-recovery preparation to perform T_1-weighted MRI. In standard protocols, the inversion time is set in order to saturate the cerebrospinal fluid (CSF) and yields a good contrast between the gray matter (GM) and the white matter (WM), for example, in the context of a diagnosis of Alzheimer's disease.[6] Thanks to a shorter inversion time, MP-RAGE allows T_1-weighted MRI of the brain with WM saturation. This latter optimization of the MP-RAGE, known as Fast Gray matter Acquisition T_1 Inversion Recovery (FGATIR), offers a good GM/WM contrast and is used to visualize the targets of deep brain stimulations (DBS).[7]

Each cycle fills a fraction of the k-space, and the contrast control is a difficult numerical problem because of coupling between cycles. In the simple case of an inversion recovery, the dependence between the time of a segment (T_S), the inversion time (T_I), the repetition time (T_R), the flip angle (α), and the number of lines acquired by segment (n) has been given by Deichmann et al.[8] They put into evidence a complex dependence between all these parameters. With this model, the inversion recovery time can be determined, but nothing guarantees that it is the best preparation module with which to achieve the desired contrast between the target tissues.

In this context, we developed a numerical framework that optimizes a preparation module composed of an arbitrary number of pulses to reach the optimal contrast between target tissues based on their relaxation times.[9] This optimization stems from an optimal control algorithm (GRAdient Ascent Pulse Engineering [GRAPE][10]), which relies on a solution of the Bloch equations and a gradient-based descent on a differentiable cost function. This numerical framework takes back the parametrization of a previous optimal control framework that optimizes delays, angles, and phases of a set of RF pulses.[11] The benefit of our method lies in the inclusion of the longitudinal steady state, which allows determination of the optimal preparation in a fast gradient echo sequence. This optimal control preparation introduces T_1- and T_2-weighted contrast in this traditionally purely T_1-weighted sequence.

Thus, this article provides a rigorous numerical framework to optimize a preparation composed of an arbitrary set of RF pulses to yield the optimal contrast between target tissues based on their relaxation times difference in an MP-RAGE sequence. To show the versatility of the proposed method, in vitro validations on tubes and in vivo acquisitions on the brain of healthy volunteer, at 3 T, are detailed. Different contrasts achievable with the proposed method are demonstrated, and analysis of the possible contrast enhancement compared with standard inversion recovery is proposed.

2 | THEORY

2.1 | Modeling of a standard T_1 MP-RAGE

The notations and notions used in this paper are first introduced through the modeling of a standard MP-RAGE acquisition scheme. For a simple inversion-recovery preparation, the cyclic nature of the sequence with no full recovery of the magnetization between each cycle leads to a stationary state. In this simple case, the stationary state only concerns the longitudinal magnetization: transverse magnetization is considered to be properly spoiled during the gradient echo readout as well as on both sides of the inversion pulse, which only exploits T_1 regrowth. The evolution of the longitudinal magnetization at different steps of a cycle of duration T_S, $M_{z,j=1,2,..4}$, is described in Figure 1. In the following, $M_{z,1}^{k+1}$ represents

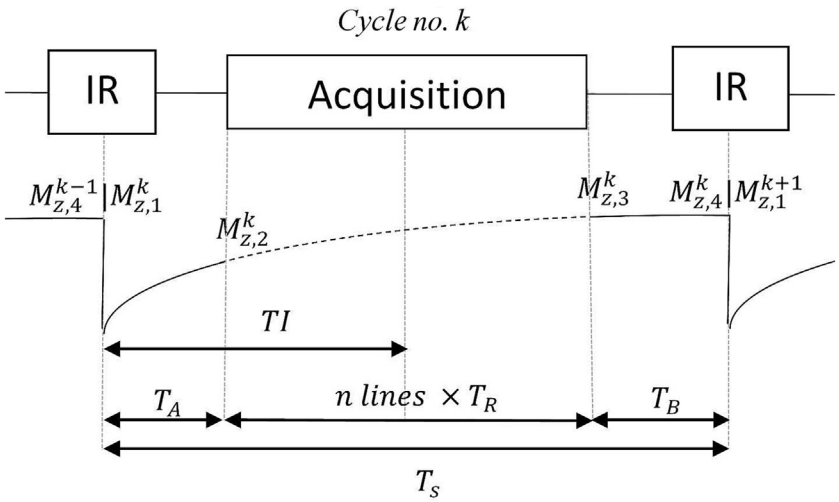

FIGURE 1 Schematic diagram of the T_1 MP-RAGE sequence. IR, inversion recovery; MP-RAGE, magnetization-prepared rapid gradient-echo.

the longitudinal magnetization straight after the inversion at the cycle k + 1. $M_{z,4}^{k}$ represents the longitudinal magnetization just before the inversion at the end of the cycle k. Below are detailed the relations between the values of the longitudinal magnetization at each step in a cycle k + 1:

$$\begin{cases} M_{z,1}^{k+1} = -eff.M_{z,4}^{k} & inversion \\ M_{z,2}^{k+1} = M_0(1-E_A) + E_A M_{z,1}^{k+1} & T_1\ regrowth \\ M_{z,3}^{k+1} = M_0^*(1-K_1^n) + K_1^n M_{z,2}^{k+1} & evolution\ during\ the\ acquisitions \\ M_{z,4}^{k+1} = M_0(1-E_B) + E_B M_{z,3}^{k+1} & T_1\ regrowth, \end{cases}$$

with $E_A = e^{-\frac{T_A}{T_1}}$, $E_B = e^{-\frac{T_B}{T_1}}$, $E_1 = e^{-\frac{T_R}{T_1}}$, and $K_1 = cos(\alpha)E_1$. T_A (ms) is the delay between the inversion pulse and the beginning of the acquisitions train, and T_B (ms) is the delay between the end of the acquisitions train and the following inversion pulse. α (radian) is the flip angle, and T_R (ms) is the time of repetition of the gradient echo scheme. n refers to the number of lines encoded per cycle. The parameter eff is the efficacy of the inversion (1 is optimal). M_0^* is the value of the steady state towards which the longitudinal magnetization would converge after a very long acquisitions train; it is related to the magnetization at thermal equilibrium M_0 by the following equation:

$$M_0^* = M_0 S_1 = M_0 \frac{1-E_1}{1-cos(\alpha)E_1}. \tag{1}$$

By iteratively inserting the previous equation in the next one, it follows that

$$M_{z,4}^{k+1} = M_0(1-E_B) + M_0^* E_B(1-K_1^n) + M_0 E_B K_1^n (1-E_A) - eff.E_A K_1^n E_B M_{z,4}^{k}. \tag{2}$$

Then, solving $M_{z,4}^{k+1} = M_{z,4}^{k}$ gives the following magnetization steady state:

$$ss = M_0 \frac{(1-E_B) + S_1 E_B(1-K_1^n) + E_B K_1^n (1-E_A)}{1 + eff.E_B K_1^n E_A}. \tag{3}$$

2.2 | OC pulse design for the magnetization preparation: the elements to be optimized

The idea is to use the full description of the magnetization dynamics described by the Bloch equations on the model of the optimal control algorithm (i.e., GRAPE). Equation (4) presents the Bloch equations in the rotating frame of angular frequency ω around the z-axis. $\Delta\omega = -\gamma B_0 - \omega$. $\boldsymbol{\omega_1} = (\omega_x, \omega_y) = -\gamma \mathbf{B_1}$. B_1 is the RF excitation field.

$$\frac{d}{dt}\begin{pmatrix} M_x \\ M_y \\ M_z \\ 1 \end{pmatrix} = \begin{pmatrix} -\frac{1}{T_2} & -\Delta\omega & \omega_y & 0 \\ \Delta\omega & -\frac{1}{T_2} & -\omega_x & 0 \\ -\omega_y & \omega_x & -\frac{1}{T_1} & \frac{M_0}{T_1} \\ 0 & 0 & 0 & 1 \end{pmatrix} \begin{pmatrix} M_x \\ M_y \\ M_z \\ 1 \end{pmatrix}, \tag{4}$$

where $\mathbf{M} = {}^t(M_x, M_y, M_z, 1)$ is the extended magnetization vector. Time is discretized so that the RF field can be considered as a piecewise constant function and the Bloch equations are integrated step by step. The RF field can be optimized as an uninterrupted field[10,12] or as a sequence of brief pulses interrupted by free evolution times.[11] The latter approach is used in this article. Parameters for a N-pulse preparation can be summed up in a vector of $N \times 2$ RF field components $\left(\omega_x^i, \omega_y^i\right)$ and $N+1$ delays τ^i. Then, we have the following relations (Equation 5):

$$\begin{gathered} \mathbf{M}_{i+1} = U_i \mathbf{M}_i \ with\ U_i = U\left(\omega_x^i, \omega_y^i, \tau^i\right) \\ \mathbf{u} = \left(\tau^0, \omega_x^1, \omega_y^1, \tau^i, ..., \omega_x^N, \omega_y^N, \tau^N\right), \mathbf{u}_i = \left(\omega_x^i, \omega_y^i, \tau^i\right), \end{gathered} \tag{5}$$

where $U_i = U(u_i)$ is the transfer matrix modeling the action of the ith pulse and the free evolution during the following delay τ^i (Figure 2). Vector $\mathbf{u}$ contains all the variables that will be optimized, as described in the following sections.

2.3 | Modeling of an arbitrary MP-RAGE with OC preparation

In the presence of a complex preparation, the ratio between the magnetization before and after the preparation is no longer constant. We assume that the effect of the preparation on the magnetization can be modeled by the aforementioned N + 1 transfer matrices, each modeling the effect of a pulse followed by a time of relaxation (Equation 6).

$$\mathbf{M}_{Out} = U_N U_{N-1} \ldots U_0 \mathbf{M}_0, \mathbf{M}_{Out} = U\mathbf{M}_{In}. \tag{6}$$

More precisely,

$$\mathbf{M}_{Out} = \begin{pmatrix} \mathcal{A}_u & \mathbf{q}_u \\ 0 & 1 \end{pmatrix} \mathbf{M}_{In}, \tag{7}$$

where $\mathbf{M}_{In}$ and $\mathbf{M}_{Out}$ are, respectively, the magnetization before and after the preparation. Considering that any transverse magnetization is adequately spoiled before and after the preparation ($M_x = M_y = 0$), it follows Equation (8). One can then retrieve the transfer relation (Equation 9).

$$\begin{pmatrix} 0 \\ 0 \\ M_{z\,Out} \\ 1 \end{pmatrix} \begin{pmatrix} A_{u\,1,1} & A_{u\,1,2} & A_{u\,1,3} & q_{u\,1} \\ A_{u\,2,1} & A_{u\,2,2} & A_{u\,2,3} & q_{u\,2} \\ A_{u\,3,1} & A_{u\,3,2} & A_{u\,3,3} & q_{u\,3} \\ 0 & 0 & 0 & 1 \end{pmatrix} \begin{pmatrix} 0 \\ 0 \\ M_{z\,In} \\ 1 \end{pmatrix} \tag{8}$$

$$M_{z\,Out} = A_{u3,3} M_{z\,In} + q_{u3}\, i.e. M_{z\,Out} = f(\mathbf{u}) M_{z\,In} + h(\mathbf{u}) \tag{9}$$

As $f(\mathbf{u})$ and $h(\mathbf{u})$ remain unchanged during each cycle, this enables updating of the previous expression (Equation 3) of steady state to a general expression (Equation 12).

$$M_{z,4}^{k+1} = M_0(1 - E_B) + M_0 S_1 E_B (1 - K_1^n) + E_B K_1^n (1 - E_A) + E_B K_1^n E_A \left(f(\mathbf{u}) M_{z,4}^k + h(\mathbf{u}) \right) \tag{10}$$

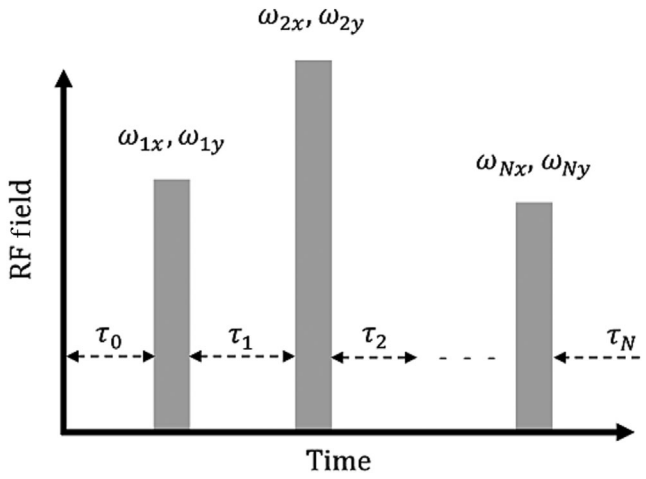

FIGURE 2 Parametrization of the preparation composed of a set of pulses.

$$ss = \frac{M_0\left[(1-E_B)+S_1E_B\left(1-K_1^n\right)+E_BK_1^n(1-E_A)\right]+E_BK_1^nE_Ah(\mathbf{u})}{1-E_BK_1^nE_Af(\mathbf{u})} \tag{11}$$

$$ss = \frac{A+\lambda h(\mathbf{u})}{1-\lambda f(\mathbf{u})} \tag{12}$$

$$A = M_0\left[(1-E_B)+S_1E_B\left(1-K_1^n\right)+E_BK_1^n(1-E_A)\right], \lambda = E_BK_1^nE_A \tag{13}$$

A and λ only depend on the acquisition parameters. $h(\mathbf{u})$ and $f(\mathbf{u})$ only depend on preparation parameters. Then, it is possible to step back until the ith excitation in a cycle and to express the signal at corresponding echo (Equation 14). For example, $j=1$ and $j=n/2$ correspond to the center of the k-space, respectively, in the case of centrally phase reordering and sequential phase reordering.

$$S_j = \left[M_0S_1+\left(\frac{ss(\mathbf{u})-(1-E_B)}{E_B}-M_0S_1\right)K_1^{-(n-j+1)}\right]sin(\alpha)e^{-\frac{TE}{T_2}} \tag{14}$$

2.4 | Description of the optimization problem

The goal is to determine the best RF field to prepare the sequence that maximizes the contrast between two target tissues in the center of the k-space, taking into account the formation of the steady state. Spins are characterized by relaxation times T_1, T_2, off-resonance $\Delta\omega = -\gamma\Delta B_0$, and equilibrium value M_0. With a N-pulse preparation whose parameters are stored in the vector $\mathbf{u}$, the contrast optimization problem can be formulated using various cost functions:

$$\left\{\min_{\mathbf{u}} C(\mathbf{u},T_R,\alpha) = \left|S_{aj}\right|_\epsilon - \left|S_{bj}\right|_\epsilon \right. \tag{15}$$

or

$$\begin{cases} \min_{\mathbf{u}} C(\mathbf{u},T_R,\alpha) = -\left|S_{bj}\right|_\epsilon \\ subject\ to\ S_{aj}=0 \end{cases}, \tag{16}$$

where $S_{a/bj}$ is the signal intensity of a tissue a, to be saturated, or a tissue b, to be maximized, after the jth gradient echo acquisition of the readout, once the steady state is reached. $\left|S_{bj}\right|_\epsilon = \sqrt[\epsilon]{S_{bj}^2+\epsilon^2} \underset{\epsilon\to 0}{\to} \left|S_{bj}\right|$ is the approximation of the absolute value to avoid the problem of non-differentiability ($\epsilon = 10^{-5}$). $\mathbf{u} \in \mathbb{R}^{N\times 3+1}$ is the optimization variables vector composed of 2N angular frequencies components $\left(\omega_i^x,\omega_i^y\right)_{1\le i\le N}$ and N + 1 delays $(\tau_i)_{0\le i\le N}$. The cost function aims at maximizing the contrast when acquiring the central line of the k-space. In our case, centric reordering is used ($j=1$). Segment duration T_S is fixed.

As a result, there follows a linear equality constraint on the delays (Equation 17). To bypass this constraint, we proceed to a change of variables, consisting of substituting $\boldsymbol{\tau} = (\tau_0,\tau_1,...,\tau_N)$ for $\boldsymbol{\lambda} = (\lambda_0,\lambda_1,...,\lambda_N)$ defined by Equation (18). This way, optimization variables λ_i are only constrained to be strictly positive. Gradient with respect to the λ_i is computed by multiplying by the Jacobian matrix $J_{\lambda(\tau)}$ (Equation 20).

$$\tau_0+\tau_1+...+\tau_N = T_S \tag{17}$$

$$\tau_i = \frac{\lambda_i}{\lambda_0+\lambda_1+...+\lambda_N}T_S, \lambda_i > 0 \tag{18}$$

$$\nabla_{C(\boldsymbol{\lambda})} = {}^t\mathcal{J}_{\boldsymbol{\tau}(\boldsymbol{\lambda})}\nabla_{C(\boldsymbol{\tau})} \tag{19}$$

$$\begin{aligned}\mathcal{J}_{\boldsymbol{\tau}(\boldsymbol{\lambda})} &= \left(\frac{\partial\tau_i}{\partial\lambda_j}\right)_{0\le i\le N, 0\le j\le N} \\ &= \frac{\delta_{ij}(\lambda_0+\lambda_1+...+\lambda_n)-\lambda_i}{(\lambda_0+\lambda_1+...+\lambda_N)^2}\end{aligned} \tag{20}$$

A constraint on the saturation of one or several tissues can be added (Equation 16). To this end, longitudinal magnetization just before the desired excitation of the gradient echo acquisition is set to zero (Equation 21). The gradient of each constraint is computed in the same manner as for the objective function.

$$M_{z,ligne\ n^o j} = M_0 S_1 + \left(\frac{ss(\mathbf{u}) - (1 - E_B)}{E_B} - M_0 S_1 \right) K_1^{-(n-j+1)} = 0 \tag{21}$$

2.5 | Problem resolution

The optimization is conducted thanks to a gradient descent algorithm structured on the model of the GRAPE algorithm. The algorithm is coded on Matlab (MathWorks Inc., Natick, MA, USA; R2019b) using the solver of the function fmincon. The solver of this constrained nonlinear optimization uses a sequential quadratic programming (SQP) method.[13] At each iteration, an approximation of the Hessian matrix is computed using the Limited-Memory Broyden–Fletcher–Goldfarb–Shanno algorithm (L-BFGS) method.[14] Analytic expression of the partial derivatives of objective and constraint functions is provided to the solver. To this end, it is necessary to differentiate the previously described steady state (Equation 12) with respect to the control field $\mathbf{u}$:

$$\nabla ss = (A + \lambda h(\mathbf{u})) \frac{1}{(1 - \lambda f(\mathbf{u}))^2} \nabla f(\mathbf{u}) + \frac{\lambda}{1 - \lambda f(\mathbf{u})} \nabla h(\mathbf{u}). \tag{22}$$

Remembering Equation (8), $f(\mathbf{u}) = {}^t\mathbf{e_z} U \mathbf{e_z}$ and $h(\mathbf{u}) = {}^t\mathbf{e_z} U \mathbf{e_0}$, where $\mathbf{e_z} = {}^t(0,0,1,0)$ and $\mathbf{e_0} = {}^t(0,0,0,1)$. Then the transfer matrix is

$$U = \begin{pmatrix} * & * & * & * \\ * & * & * & * \\ * & * & f(\mathbf{u}) & h(\mathbf{u}) \\ 0 & 0 & 0 & 1 \end{pmatrix}. \tag{23}$$

For an arbitrary N-pulse preparation, $U = U_N \ldots U_1 U_0$, $U_i = U(u_i)$ is the transfer matrix modeling the effect of ith pulse and delay whose parameters are regrouped into the vector $\mathbf{u}_i = (u_{i1}, u_{i2}, u_{i3})$. So

$$\nabla_{u_{ij}} f = {}^t\mathbf{e_z} \frac{\partial U}{\partial u_{ij}} \mathbf{e_z}, \nabla_{u_{ij}} g = {}^t\mathbf{e_z} \frac{\partial U}{\partial u_{ij}} \mathbf{e_0}. \tag{24}$$

At this point, we have expressed the steady state and its partial derivatives with respect to the preparation scheme parameters. With the chain rule derivation, we can derive any functions that are composite functions of $ss(\mathbf{u})$.

Prior to the gradient descent, the cost function and constraint functions are evaluated on a large number of initializations (in the range of 1000–3000). A restricted number of initializations that minimize the cost function is first selected among those that respect the constraints with a tolerance of 10^{-4} and then among the other ones until there are 20 starting points for the gradient descent. Maximum iterations are fixed to 1000 and step tolerance to 10^{-6}.

3 | MATERIALS AND METHODS

3.1 | Materials

Experiments were performed at 3 T (MAGNETOM Vida, Siemens Healthcare, Erlangen, Germany).

To perform in vitro and in vivo validations, a sequence was developed based on a three-dimensional (3D) FLASH sequence implementing a segmented acquisition with a phase-centric reordering scheme. Preparation modules were composed, when applicable, of standard pulses: inversion recovery with an adiabatic hyperbolic secant pulse of 10 ms, 90° excitation pulses with rectangular pulses of 0.8 ms, and refocusing pulses with adiabatic full passages of 10 ms. The use of 3D adiabatic pulses provides robustness against B_1 variations, but also good efficiency over a large bandwidth to counter B_0 inhomogeneities. The dephasing of the magnetization in the transverse plane during free precession due to the B_0 inhomogeneities is not considered in the present optimization. According to the preparation results, a refocusing pulse (180^{o}_{y}) may need to be added to preserve phase coherence, in particular between two 90° excitation pulses. Thus, during the multipulse preparation schemes, the 180° refocusing pulse canceled the dephasing of the transverse magnetization at the origin of the $T_{2}*$ decay, ensuring a T_2 decay of the transverse magnetization in accordance with the modelization.

3.2 | Acquisition parameters

For the in vivo and in vitro experiments, the acquisition parameters are listed in Table 1. As the number of lines acquired per segment was fixed to 64, four cycles were necessary to fill a k-space slice for a matrix of 256 × 256. Centric reordering was chosen, meaning that the cost function was evaluated at the first echo, which corresponds to the four central lines of the k-space. This allows more flexible contrast.[15,16] T_R was fixed to the minimum possible in the sequence ($T_R = 6$ ms). The flip angle was set to 12° to achieve the maximum signal level without impacting too much the spatial resolution due to the signal evolution during the acquisitions train.

3.3 | Phantom experiments

The optimization algorithm was applied in vitro for a set of 12 test tubes (Spin Safety), with different T_1 and T_2 relaxation times. T_1 relaxation times were estimated with several MP-RAGE acquisitions employing different inversion times from 60 to 600 ms. T_2 relaxation times were also estimated with several MP-RAGE acquisitions by using different T_2Prep (T_2Prep with different echo times from 15 to 150 ms). The estimated T_1 and T_2 relaxation times are presented in Table 2 for the 12 tubes, numbered from 1 to 12. Based on these measures, preparation schemes were optimized using the proposed framework. To emphasize the versatility of our method, preparations were optimized to reach the optimal contrast between different pairs of targeted tubes: tubes no. 7 and no. 12, no. 7 and no. 11, and no. 9 and no. 11. T_1/T_2 (ms) for tubes no. 7, no. 9, no.

TABLE 1 Acquisition parameters for in vitro and in vivo acquisitions.

Parameters	In vitro	In vivo
Flip angle/TR	12°/6 ms	12°/6 ms
Time of a segment	1500 ms/2000 ms(1)/3000 ms(2)	2000 ms/5000 ms(3)
Phase-encoding scheme	*Reordered*	*Reordered*
Number of lines per cycle	64	64
Number of dummy cycles	4	4
Matrix	256 × 256 × 4	256 × 256 × 32
Number of accumulations	8	1
FOV/slice thickness	300 × 300 mm/5 mm	300 × 300 mm/5 mm
		256 × 256 mm/4 mm(3)
Time of acquisition	4 min/5 min 20 s(1)/8 min(2)	4 min 10 s/11 min(3)

Notes: In some cases, segment durations were lengthened in order to have a better signal level: (1) the double saturations of tubes no. 9 and no. 11, as well as tubes no. 6 and no. 11; (2) the double saturation of tubes no. 7 and no. 11; (3) the double saturation of the white matter and the gray matter. For series of acquisitions with decreasing segment durations, the times of the acquisition are not detailed in the table.
Abbreviations: FOV, field of view; TR, repetition time.

TABLE 2 Measured relaxation times of Spins Safety tubes with the 95% confidence interval.

Tube no.	1	2	3	4	5	6	7	8	9	10	11	12
T_2 (ms)	–	–	–	–	–	10 ± 4	34 ± 5	–	54 ± 4	–	74 ± 4	48 ± 3
T_1 (ms)	67 ± 1	58 ± 1	59 ± 1	58 ± 1	106 ± 3	74 ± 3	483 ± 6	181 ± 4	633 ± 5	300 ± 4	762 ± 7	770 ± 14

11, and no. 12 are 34/485, 54/633, 74/762, and 48/770, respectively. These samples were chosen to evaluate the performance of the proposed preparation schemes in various situations: significant differences in T_1 and T_2 (7/12), large T_2 difference (7/11), and small T_1 difference (9/11). For each of the pairs of tubes mentioned above, two cases were considered. In the first case, the objective was to enhance the signal of the tube with the shortest relaxation times while saturating the other one. In the second case, the objective was to enhance the signal of the tube with the longest relaxation times while saturating the other one, that is, the opposite. For each case, the optimization was performed for a one-pulse preparation (1p.-preparation) and a preparation limited to two preparation pulses (2p.-preparation). In summary, the following cost function C was used:

$$C = -|S_b| \; subject\; to\; S_a = 0, \tag{25}$$

where S_b is the normalized intensity in the center of the k-space for the tube which signal is to be maximized, and S_a is the normalized intensity in the center of the k-space for the tube that must be nulled. Here, the segment duration was fixed to 1.5 s.

Then we investigated the possibilities of enhancing the signal of the tube of the shortest T_2 and T_1 when the segment duration decreases. To this end, for segment durations from 1.5 to 0.75 s (i.e., 1.5, 1.25, 1, and 0.75 s), sequences with a 1p.-preparation and a 2p.-preparation were optimized.

Finally, more difficult contrasts, consisting of simultaneously saturating two tubes and maximizing a third one, were targeted. This was conducted on tubes no. 6, no. 7, and no. 11, which have relaxation times distributed over a large range of values. We considered the three possibilities for a tube signal to be enhanced. For this challenging contrast objective, up to three excitation pulses for the preparation (3p.-preparation) was permitted. The best numerical solutions in terms of signal difference were selected.

The duration of each segment was fixed to 1.5 s to maintain a reasonable acquisition time. This has major implications in terms of signal level. Consequently, for difficult contrast, during the double saturation of tubes no. 6 and no. 11, no. 6 and no. 7, and no. 7 and no. 11, T_S was lengthened to 3, 3, and 2 s, respectively.

3.4 | In vivo experiments

For in vivo experiments conducted on the healthy brain of a volunteer, the proposed method was applied to control the contrast between the GM, the WM, and the CSF. T_1 and T_2 relaxation times at 3 T, as well as proton density (PD), were assessed based on the literature.[17,18] The values retained for T_1/T_2/PD for the GM, the WM, and CSF were 1450 ms/96 ms/0.75, 923 ms/70 ms/0.65, and 4200 ms/2000 ms/1, respectively. Optimal 1p.-preparation and 2p.-preparation in order to saturate the WM and enhance the GM, like in a FGATIR sequence, were targeted first. T_S was fixed to 2 s. Then the possibility of enhancing the GM while saturating both the CSF and the WM, like in a double inversion recovery (DIR) sequence,[19] with a 3p.-preparation, was computed and applied. For the double saturation of the WM and the CSF, T_S was fixed to 5 s. For in vivo experiments, acquisition times ranged from 4 min 10 s to 11 min.

The protocol was approved by the Ethic Committee LYON-EST and ensured that informed consent was provided by each of the volunteers.

3.5 | Analysis

The performances of the different solutions were compared quantitatively using the signal-to-noise ratio (SNR) and the contrast-to-noise ratio (CNR). SNR is computed as the mean signal in a region divided by the standard deviation of the background noise. CNR is computed as the signal intensity difference between two regions divided by the standard deviation of the background noise.

4 | RESULTS

4.1 | Phantom experiments: numerical results

In this section, the numerical results obtained with the proposed optimization method are presented. Table 3 details the numerical results for the optimal 1p.-preparation and 2p.-preparation modules to enhance the contrast between tubes no. 11 and no. 7. The numerical results for the other pairs of tubes are detailed in Section 6. In the case of the 1p.-preparation, the optimal preparation resulted in a standard inversion recovery with different inversion times. In the case of the 2p.-preparation, the optimal preparation often resulted in the following scheme:

TABLE 3 Optimized parameters for contrast problems consisting of saturating tube no. 11 and maximizing tube no. 7 and inversely in the case of a 1p.-preparation and a 2p.-preparation. Time (s) corresponds to the duration of the optimization.

Contrast between tubes no. 7 and no. 11			
Tube max/min, N pulses	**Preparation module**	**Signal at first echo $\times 10^{-2}$**	**Time (s)**
7/11, 1 pulse	$713\,\text{ms} - 180^{\circ}_{x} - 403\,\text{ms} - acq.$	$S_7 = +3,9 \mid S_{11} = +0.0$	22.3
7/11, 2 pulses	$813\,\text{ms} - 91^{\circ}_{x} - 41\,\text{ms} - 86^{\circ}_{x} - 262\,\text{ms} - acq. -$	$S_7 = +5,5 \mid S_{11} = +0.0$	46.1
11/7, 1 pulse	$817\,\text{ms} - 180^{\circ}_{x} - 299\,\text{ms} - acq.$	$S_7 = -0,1 \mid S_{11} = -3.3$	17.0
11/7, 2 pulses	$971\,\text{ms} - 91^{\circ}_{x} - 40\,\text{ms} - 87^{\circ}_{x} - 106\,\text{ms} - acq.$	$S_7 = -0,1 \mid S_{11} = -5.0$	60.8

TABLE 4 Optimized parameters for contrast problems consisting of maximizing one of the tubes no. 6, no. 7, or no. 11, while saturating both of the other ones. For the enhancement of tube no. 6, $T_S = 2\,\text{s}$; otherwise, $T_S = 3\,\text{s}$.

Tube max/min	**Preparation module**	**Signal at first echo (10^{-2})**	**Time (s)**
6/7, 11	$729\,\text{ms} - 90^{o}_{x} - 41\,\text{ms} - 86^{o}_{x} - 606\,\text{ms} - 180^{o}_{x} - 256\,\text{ms} - acq. -$	$S_6 = 15.4 \mid S_7 = +0.0 \mid S_{11} = -0.0$	211
11/6, 7	$2346\,\text{ms} - 91^{o}_{x} - 33\,\text{ms} - 86^{o}_{x} - 191\,\text{ms} - 179^{o}_{x} - 46\,\text{ms} - acq. -$	$S_6 = -0.0 \mid S_7 = +0.0 \mid S_{11} = 5.7$	136
7/6, 11	$2009\,\text{ms} - 180^{o}_{x} - 557\,\text{ms} - 180^{o}_{x} - 49\,\text{ms} - acq. -$	$S_6 = -0.0 \mid S_7 = -4.6 \mid S_{11} = -0.0$	143

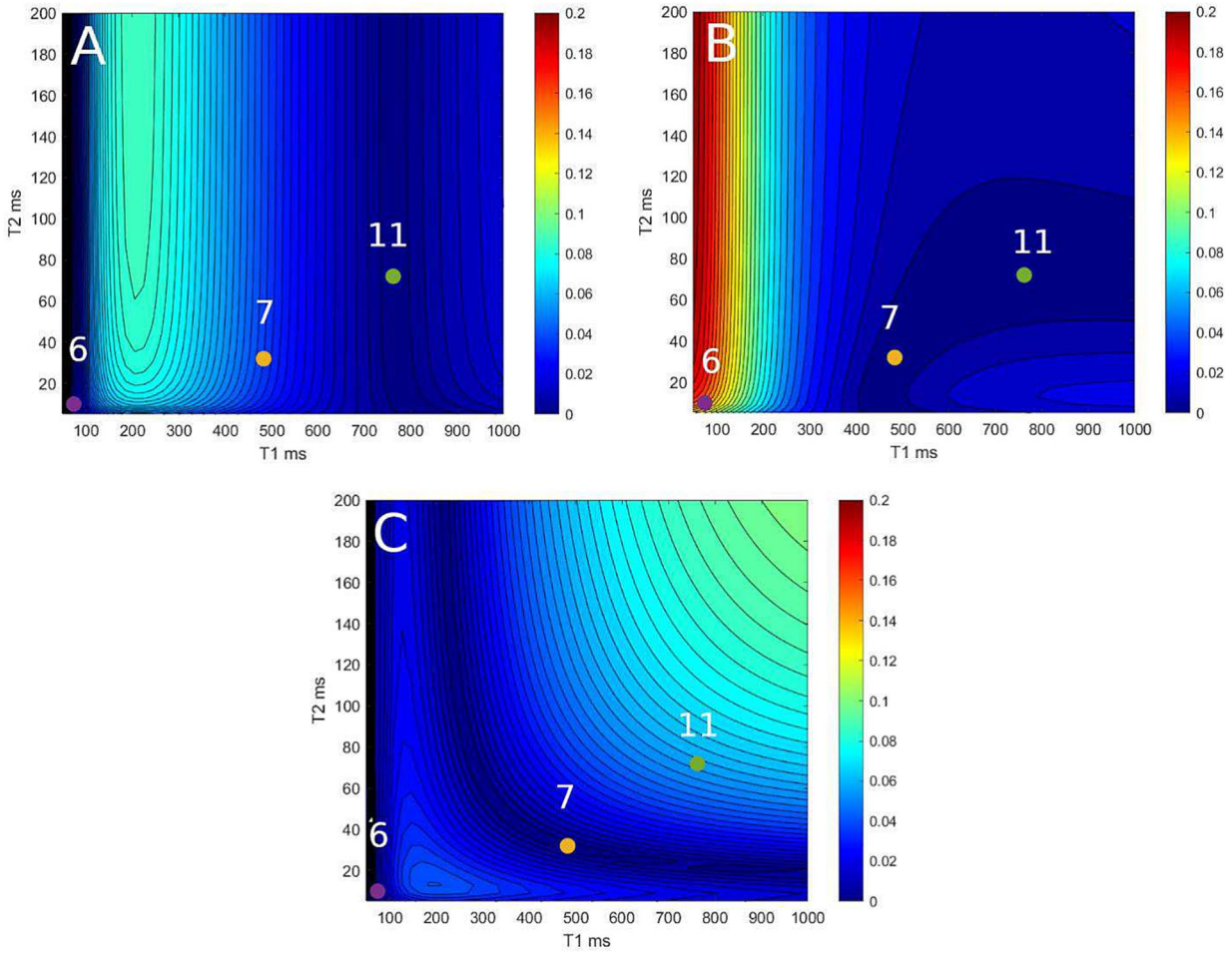

FIGURE 3 Examples of cartographies that give the normalized signal intensity in the center of the k-space as a function of T_1/T_2 values for the different preparation schemes. (A) Saturation of tubes no. 11 and no. 6, maximization of tube no. 7 (DIR). (B) Saturation of tubes no. 7 and no. 11, maximization of tube no. 6 (3p.-OCPrep). (C) Saturation of tubes no. 6 and no. 7, maximization of tube no. 11 (3p.-OCPrep). DIR, double inversion recovery; OC, optimal control.

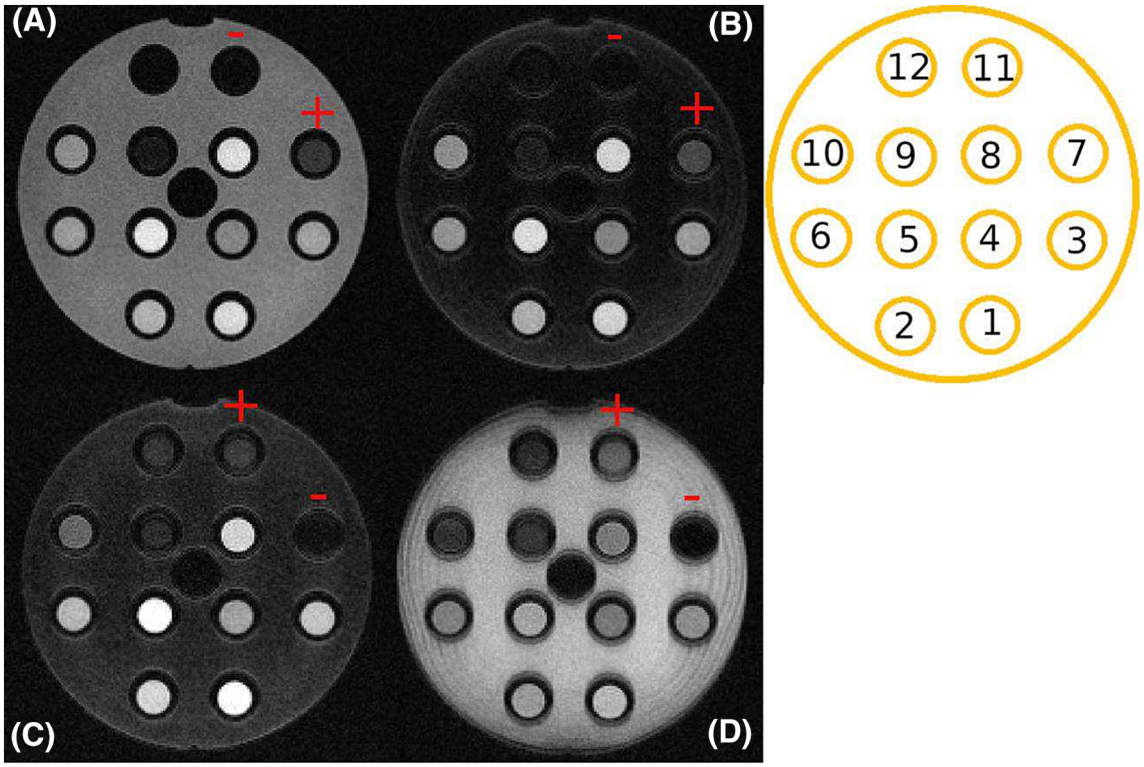

FIGURE 4 Four MP-RAGE acquisitions with the optimal preparations focusing on the contrast between tubes no. 11 and no. 7. Corresponding numbers of the tubes are indicated on the right side. In (A) and (B), the signal of tube no. 7 is maximized (+), while the signal of tube no. 11 is saturated (−), with standard inversion preparation and 2p.-OCPrep, respectively. In (C) and (D), the signal of tube no. 11 is maximized (+), while the signal of tube no. 7 is saturated (−), respectively, with standard inversion preparation and 2p.-OCPrep. (A) and (B) are displayed with the same window level, as well as (C) and (D). Note the blurring in the phase direction (vertical direction), as well as artifacts in the form of concentric rings, especially in (D). The blurring may be attributed to the rapid evolution of the signal during the filling of the lines of the k-space, leading to a widening of the PSF. Concentric rings may be correlated to an imperfect refocusing of the transverse magnetization during the multipulse schemes, especially around the air/liquid interface, where B_0 homogeneities are more important. This is more visible when the last delay of relaxation before the acquisitions is short. MP-RAGE, magnetization-prepared rapid gradient-echo; OC, optimal control; PSF, point spread function.

TABLE 5 CNR measured between the tube to be maximized (bold numbers) and the tube to be nulled for the preparations composed of one excitation pulse and two excitation pulses. CNR is computed as $\frac{I_{max}-I_{min}}{\sigma}$, where σ is the standard deviation in the surrounding background.

Tubes	7/11	11/7	7/12	12/7	9/11	11/9
1 pulse	10.8	9.0	9.7	7.4	2.3	2.4
2 pulses	15.9	20.2	7.1	12.9	5.2	7.0

Abbreviation: CNR, contrast-to-noise ratio.

TABLE 6 CNR enhancement with a 2p.-preparation compared with standard inversion recovery for different segment durations (T_S). The tube to be maximized is in bold.

Tubes	7/11	7/12	9/11
$T_S = 1500$ ms	43%	−17%	90%
$T_S = 1250$ ms	62%	−9%	24%
$T_S = 1000$ ms	101%	20%	306%
$T_S = 750$ ms	163%	68%	499%

Abbreviation: CNR, contrast-to-noise ratio.

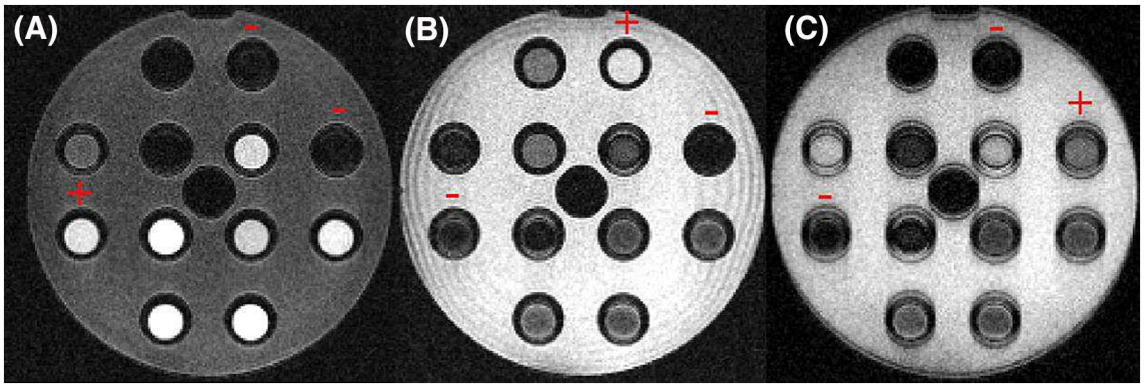

FIGURE 5 MP-RAGE acquisitions with the optimal preparations focusing on the double saturations of two tubes. (A) Double saturation of tubes no. 7 and no. 11, enhancement of tube no. 6 (3p.-OCPrep). (B) Double saturation of tubes no. 6 and no. 7, enhancement of the tube no. 11 (3p.-OCPrep). (C) Double saturation of tubes no. 6 and no. 11, enhancement of tube no. 7 (DIR). DIR, double inversion recovery; MP-RAGE, magnetization-prepared rapid gradient-echo; OC, optimal control.

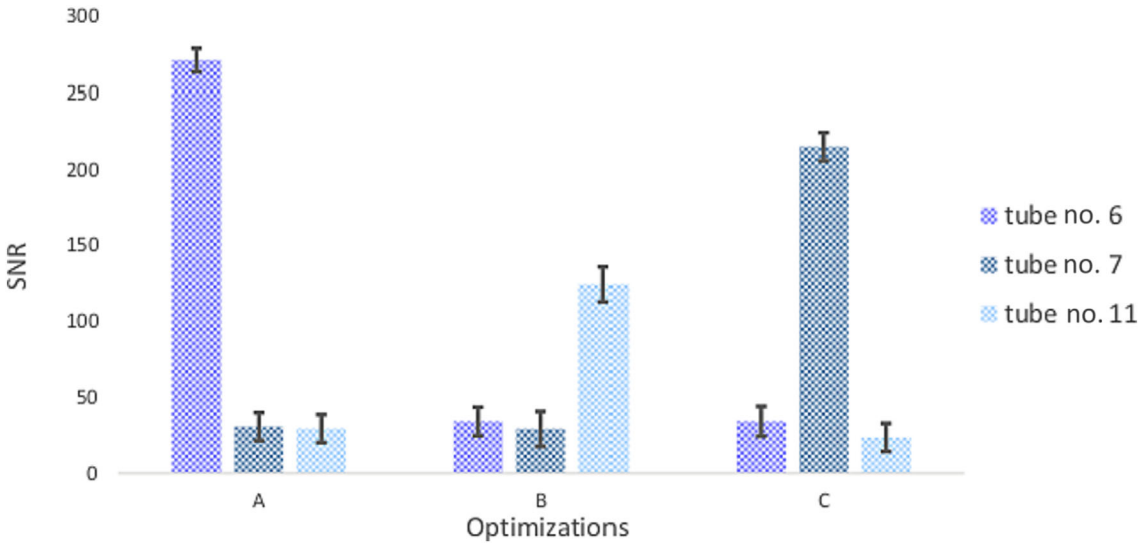

FIGURE 6 Signal-to-noise ratio (SNR) measured in tube no. 6, no. 11, and no. 7 for the three different optimizations, (A), (B), and (C). (A) Double saturation of tubes no. 7 and no. 11, enhancement of tube no. 6. (B) Double saturation of tubes no. 6 and no. 7, enhancement of tube no. 11. (C) Double saturation of tubes no. 6 and no. 11, enhancement of tube no. 7.

TABLE 7 Optimized parameters for contrast problems on the brain. For single saturation of the WM segment the duration is fixed to 2 s; for double saturation of the GM and CSF the segment duration is fixed to 5 s.

Preparation module		Signal at first echo (10^{-2})	Time (s)
Saturation of the WM and enhancement of the GM			
1 pulse	$1107\,\text{ms} - 180^{\circ}_{x} - 509\,\text{ms} - acq.$	$S_{GM} = 1.5 \mid S_{WM} = -0.0$	20.8
2 pulses	$1233\,\text{ms} - 92^{\circ}_{x} - 32\,\text{ms} - 93^{\circ}_{x} - 363\,\text{ms} - acq.$	$S_{GM} = 1.6 \mid S_{WM} = -0.0$	28.6
Saturation of the WM and the CSF, enhancement of the GM			
3 pulses	$1919\,\text{ms} - 86^{\circ}_{x} - 317\,\text{ms} - 79^{\circ}_{x} - 1830\,\text{ms} - 180^{\circ}_{x} - 550\,\text{ms} - acq.$	$S_{GM} = -2.7 \mid S_{WM} = -0.2 \mid S_{CSF} = -0.2$	81.7

Abbreviations: CSF, cerebrospinal fluid; GM, gray matter; WM, white matter.

$$delay0 - 90^{o}_{x} - delay1 - 90^{o}_{x} - delay2 - acquisitions,$$

referred to as 2p.-OCPrep, except that the flip angles were not always exactly 90° but lay between 86° and 92°. This preparation used, successively, the difference in T_2 and T_1 to increase the signal difference between the two tubes. Compared with the standard inversion, this preparation showed a benefit for pairs of tubes that had an important T_2 difference or a poor T_1 difference, that is, the pairs 7/11 and 9/11. For these two pairs, signal difference increased by at least 40% with 2p.-OCPrep compared with standard inversion.

Regarding the impact of the segment duration, the results provided evidence of a benefit of the 2p.-preparation over standard inversion recovery that was greater as the segment duration decreased. This was particularly the case for tubes no. 7 and no. 12, for which the 2p.-preparation gave a signal difference equivalent to the inversion when $T_S = 1.5$ s, whereas the 2p.-preparation provided a signal difference enhancement of 35% when $T_S = 0.75$ s. The results are presented in detail in Section 6.

Table 4 presents the numerical results for the enhancement of one of the tubes, no. 6, no. 7, or no. 11, while saturating the other two tubes. Figure 3 presents the normalized signal intensity in the center of the k-space as a function of T_1/T_2 values for the different preparation schemes. This enables visualization of the level of signal for tissues over a large range of T_1 and T_1, not only those targeted in the optimization, for the current preparations. Concerning the saturation of tubes no. 11 and no. 6, the preparation resulted in a DIR. For the saturation of tubes no. 7 and no. 6, then no. 7 and no. 11, the preparation was close to the following scheme:

$$delay0 - 90^{o}_{x} - delay1 - 90^{o}_{x} - delay2 - 180^{o}_{x} - delay3 - acquisitions,$$

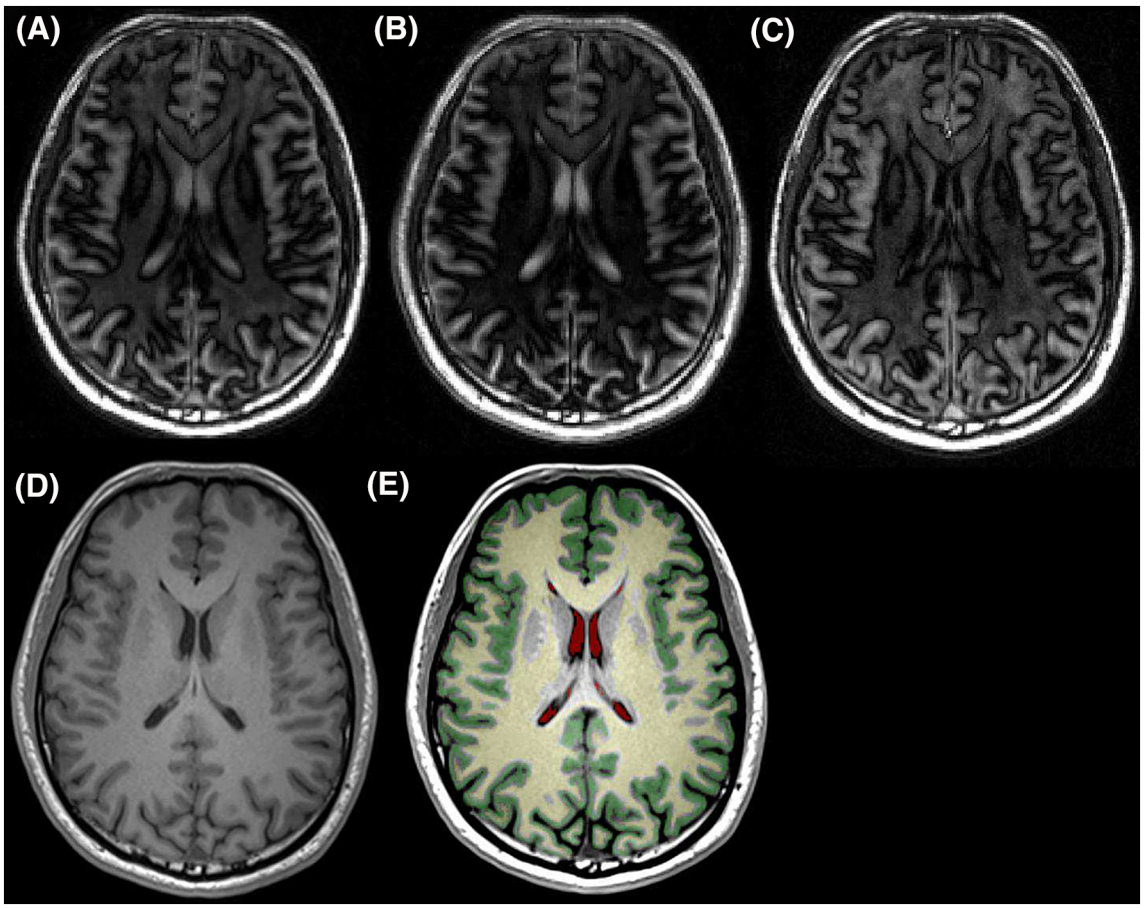

FIGURE 7 MP-RAGE acquisition with optimal preparations focusing on the contrast between WM, GM, and CSF (A–C). (D) Standard MP-RAGE from the clinical protocol. (E) Segmentations of the regions of interest, which are the WM (yellow), the GM (green), and the CSF (red). (A) Acquisition with the optimal 1p.-preparation aiming at saturating the WM and enhancing the GM. (B) Acquisition with the optimal 2p.-preparation aiming at saturating the WM and enhancing the GM. (C) Optimal 3p.-preparation aiming at saturating the WM and the CSF and enhancing the GM. (D) Standard IR MP-RAGE optimized with the protocol in order to saturate the CSF. CSF, cerebrospinal fluid; GM, gray matter; IR, inversion recovery; MP-RAGE, magnetization-prepared rapid gradient-echo; WM, white matter.

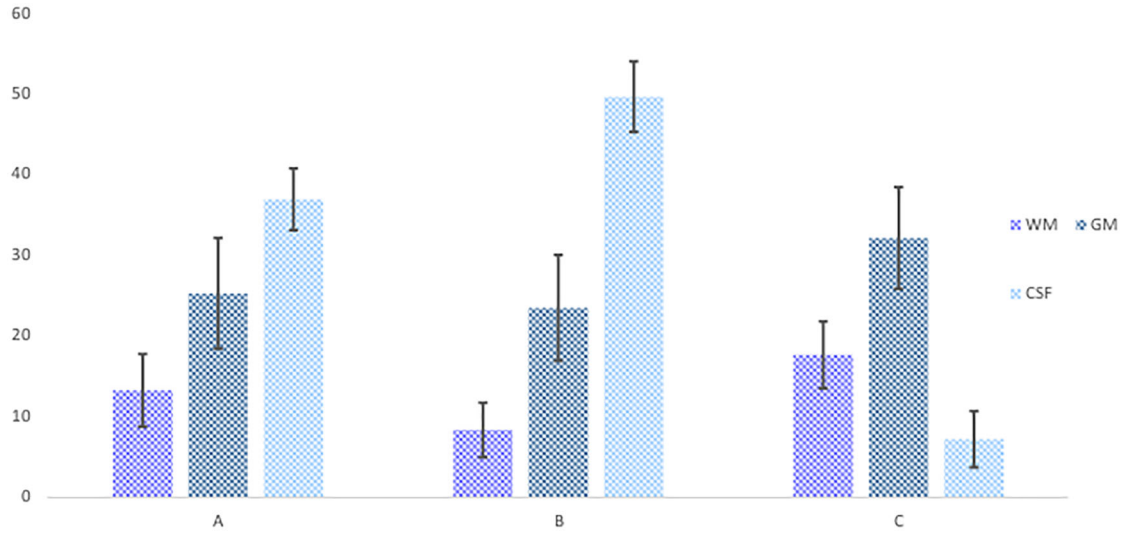

FIGURE 8 Signal-to-noise ratio measured in the regions of interest (mean +/− standard deviation), which are the WM, the GM, and the CSF for the three different optimizations (A, B, and C). (A) Saturation of the WM and enhancement of the GM with a 1p.-preparation. (B) Saturation of the WM and enhancement of the GM with a 2p.-preparation. (C) Double saturation of the WM and the CSF and enhancement of the GM, with a 3p.-preparation. CSF, cerebrospinal fluid; GM, gray matter; WM, white matter.

referred to as 3p.-OCPrep. For the three optimizations, the normalized signal intensity of the tube to be enhanced is low, except when seeking to enhance tube no. 6 (of shorter T_1 and T_2). In this case, the normalized signal intensity of the tube to be enhanced is approximately three times higher than in the two other optimizations. For the latter, the segment duration was lengthened from 2 to 3 s to improve the normalized signal intensity of the tube to be enhanced.

4.2 | Phantom experiments: experimental results

Figure 4 displays the four acquisitions with respect to the desired contrast between tubes no. 7 and no. 11; the other acquisitions are presented in Section 6. Table 5 shows the CNR for the three pairs of tubes numbered 7/11, 7/12, and 9/11. The CNR was enhanced with 2p.-OCPrep compared with standard inversion recovery, except for the enhancement of tube no. 7 while saturating tube no. 12. However, for this latter case, the numerical simulation predicted an equivalent signal difference for the two magnetization preparation solutions.

Table 6 shows the CNR enhancement with a 2p.-preparation compared with the standard inversion when seeking to enhance the tube of the shortest T_1 and T_2 for the different segment durations. As expected for the pairs of tubes numbered 7/11 (large T_2 difference) and 9/11 (small T_1 difference), the CNR was improved with 2p.-OCPrep compared with standard inversion recovery, especially for short acquisition times (short segment duration). The improvement ranged from 46% to 499%. For the pair of tubes numbered 7/12, which have a significant difference both in T_1 and in T_2, an improvement in CNR was only observed for the two shortest segment durations (1 and 0.75 s). The corresponding acquisitions are presented in on Section 6.

Figure 5 displays the acquisitions with the optimal preparations focusing on three different cases: (A) saturation of tubes no. 7 and no. 11, maximization of tube no. 6; (B) saturation of tubes no. 7 and no. 6, maximization of tube no. 11; and (C) saturation of tubes no. 11 and no. 6, maximization of tube no. 7. Figure 6 presents the SNR for the three tubes numbered 6, 7, and 11 in the three different cases A, B, and C. For all three cases, the tubes to be saturated had a signal intensity that did not exceed 25% of the average noise intensity. However, in good agreement with the numerical simulations, the signal intensity of the tube to be maximized was low, except for tube no. 6.

4.3 | In vivo brain contrast optimization: numerical results

Table 7 presents the numerical results for the different contrast objectives on the healthy brain between the GM, the WM, and the CSF.

With respect to the saturation of the WM and enhancement of the GM, the 1p.-preparation resulted in standard inversion recovery, while the 2p.-preparation resulted in 2p.-OCPrep. These two preparations gave similar results in terms of normalized signal difference between the GM and the WM.

The 3p.-preparation module targeting maximization of the GM and saturation of both the WM and the CSF resulted in 3.p.-OCPrep.

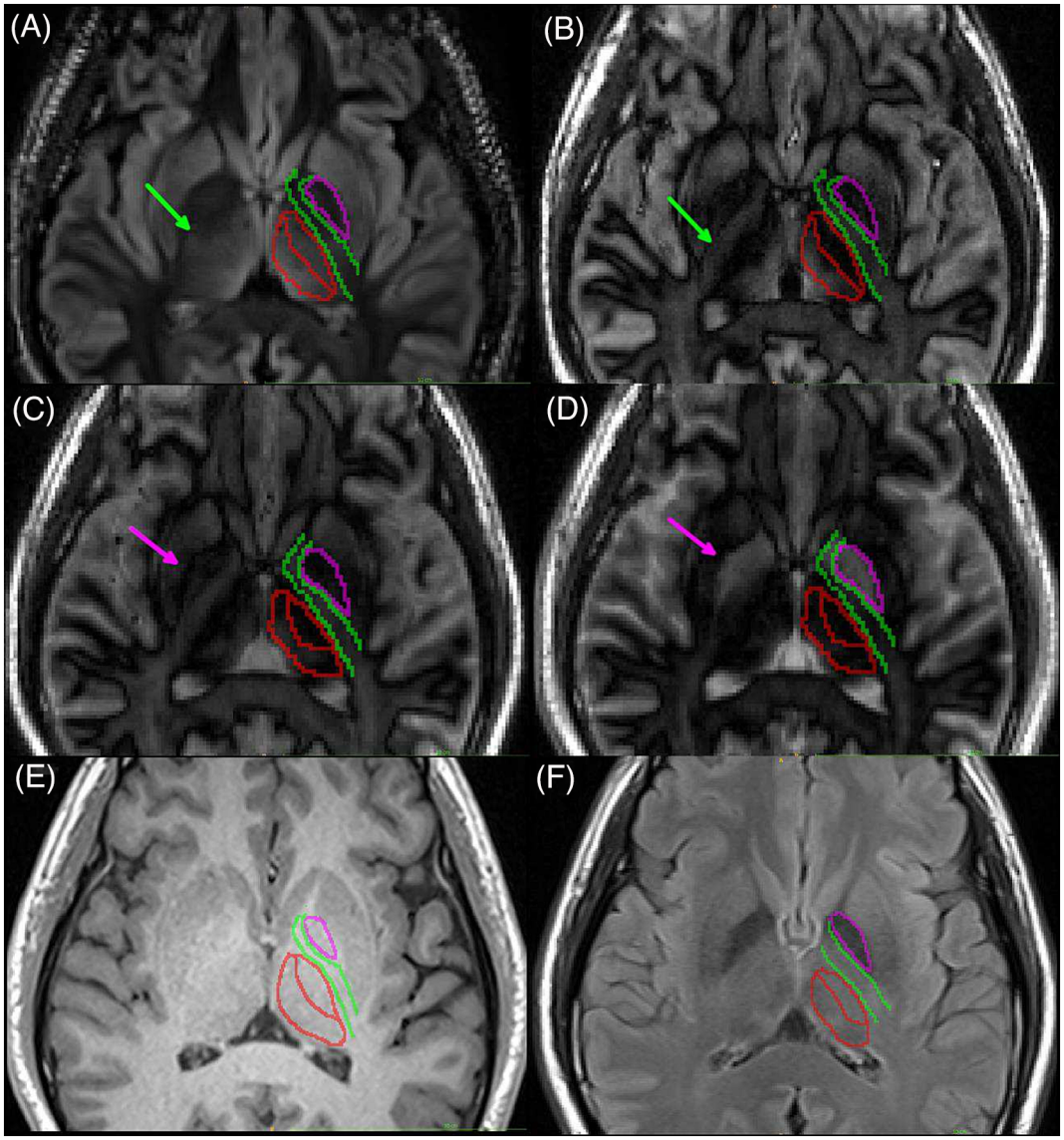

FIGURE 9 Comparison of the OC MP-RAGE acquisitions with standard clinical sequences zoomed in on the area of the deep brain structures. (A) Standard DIR-TSE with WM and CSF saturation. (B) 3p.OC-Prep with WM and CSF saturation. (C) 1p.OC-Prep with WM saturation, similar to the standard FGATIR (simple IR). (D) 2p.OC-Prep with WM saturation and GM enhancement. (E) Standard T_1-weighted MP-RAGE. (F) Standard T_2-weighted FLAIR. (B), (D), and (F) are mainly T_1-weighted, whereas (A), (C), and (E) are T_2 or mixed T_1/T_2-weighted. Deep brain structures are surrounded: in purple for the globus pallidus, in green for the internal capsule (WM structure containing axons), and in red for different thalamus regions of the thalamus (ventral vs. lateral and anterior). From the comparison between (A) and (B), we notice that 3p.OCPrep saturates less of the WM but enhances the short T_2 components in the WM that correspond to the axons; in particular, the internal capsule is clearly visible (green arrow). From the comparison between (C) and (D), it can be stated that 2p.OC-Prep MP-RAGE saturates the WM and enhances the signal of the globus pallidus (purple arrow) that is possible only using T_2 differences, because the WM and the GP share approximatively the same T_1. Finally, (E) and (F) are displayed as reference sequences for the deep brain structures imaging. Note the saturation of the globus pallidus whose T_2 is shorter that the T_1 of the WM. CSF, cerebrospinal fluid; DIR, double inversion recovery; FGATIR, Fast Gray Matter Acquisition Inversion Recovery; FLAIR, fluid-attenuated inversion recovery; IR, inversion recovery; MP-RAGE, magnetization-prepared rapid gradient-echo; OC, optimal control; TSE, turbo spin-echo; WM, white matter.

4.4 | In vivo brain contrast optimization: experimental results

Figure 7 presents the MP-RAGE acquisitions with the optimal 1p.-preparation and 2p.-preparation in order to saturate the WM and enhance the GM, as well as the optimal 3p.-preparation in order to saturate both the CSF and WM and enhance the GM. Figure 8 shows SNR for the segmented WM, GM, and CSF regions. Concerning saturation of the WM and maximization of the GM, the 2p.-preparation gave a CNR that was 25% higher compared with the standard 1p.-preparation. Indeed, the 2p.-preparation was able to produce better saturation of the WM. Concerning the double saturation of the WM and the CSF, the SNR for each of the CSF and the WM was significantly lower than the SNR of the GM. The saturation of the CSF was more pronounced.

5 | DISCUSSION AND CONCLUSION

This article gives a mathematical framework to optimize a preparation inside an MP-RAGE sequence in order to enhance the contrast between target tissues based on their relaxation times. This framework optimizes a set of angles and delays for the preparation module taking into account the formation of the steady state. It shows the potential benefit of a more complex preparation compared with standard inversion recovery for specific target tissues and a given segment duration. In addition, this framework computes nonintuitive preparations to achieve challenging contrasts, like the simultaneous saturation of two tissues in an MP-RAGE sequence. The proposed preparations illustrate that hybrid weighting can be achieved.

When the duration dedicated to the preparation is sufficiently long, the optimization converges toward preparations composed of nearly 90° and 180° pulses. In this way, the preparation successively uses T_2 and T_1 decays to create contrast. For single saturation, and especially for short segment durations, the algorithm proposes a preparation referred to as 2p.-OCPrep instead of standard inversion recovery. For the double saturations, the algorithm usually results in a DIR or 3p.-OCPrep.

The 2p.-OCPrep preparation is close to a T_2Prep,[20,21] with the difference being that the second 90° stores the magnetization along the negative z-axis, leading to an inversion of the magnetization. To that extent, this preparation is close to a $T_2Prep-IR$, in which the final inversion would immediately follow the last 90° pulse.[22,23] $T_2Prep-IR$ is commonly used in angiography to differentiate oxygenated from deoxygenated blood that share approximatively the same T_1[24] but different T_2 because of the dependence on oxygenation.[25] In our case, 2p.-OCPrep displays a benefit over standard inversion recovery when T_2 difference is significant compared with T_1 difference, or when T_1 is too long compared with the time dedicated to the preparation.

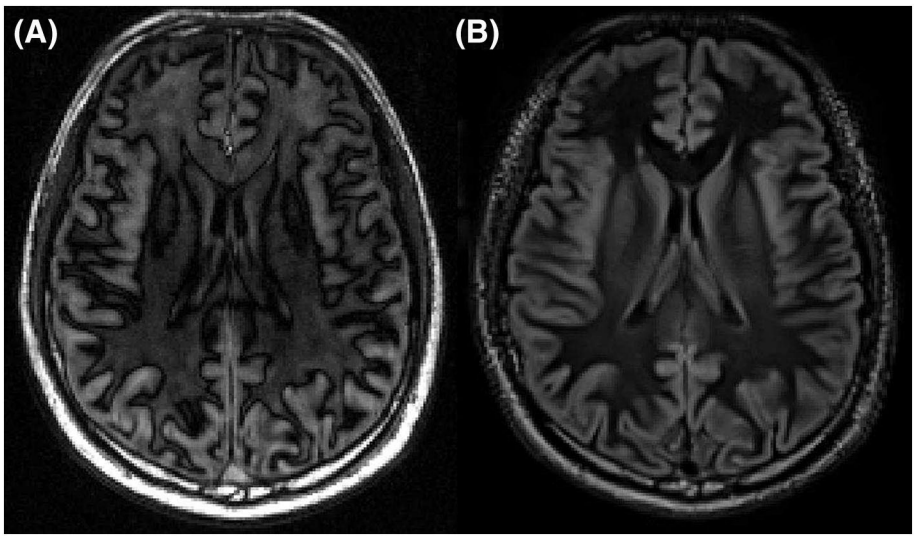

FIGURE 10 (A) 3p.-OCPrep MP-RAGE, (B) DIR TSE. For the DIR, the times of inversion $T_{I_1} = 3400$ ms and $T_{I_2} = 325$ ms came from Wattjes et al.[31] The voxel size is $1 \times 1 \times 4$ mm^3, and the matrix size is $256 \times 256 \times 32$. The effective echo time is 198 ms. The time of acquisition is approximately 6 min. The DIR TSE images were automatically registered to fit the good position and orientation of the slices of the previous 3p.-OCPrep MP-RAGE. In the 3p.-OCPrep MP-RAGE image, the WM is less saturated, especially in the frontal area; the preparation enhances the short T_2 components of the WM contrary to the DIR-TSE. As a side effect, inhomogeneities of the WM and bundles of axons are enhanced (see Figure 9A,B). Also, a dark outline surrounds the GM as an effect of the differences of phases between the WM and the GM signal. DIR, double inversion recovery; GM, gray matter; MP-RAGE, magnetization-prepared rapid gradient-echo; OC, optimal control; TSE, turbo spin-echo; WM, white matter.

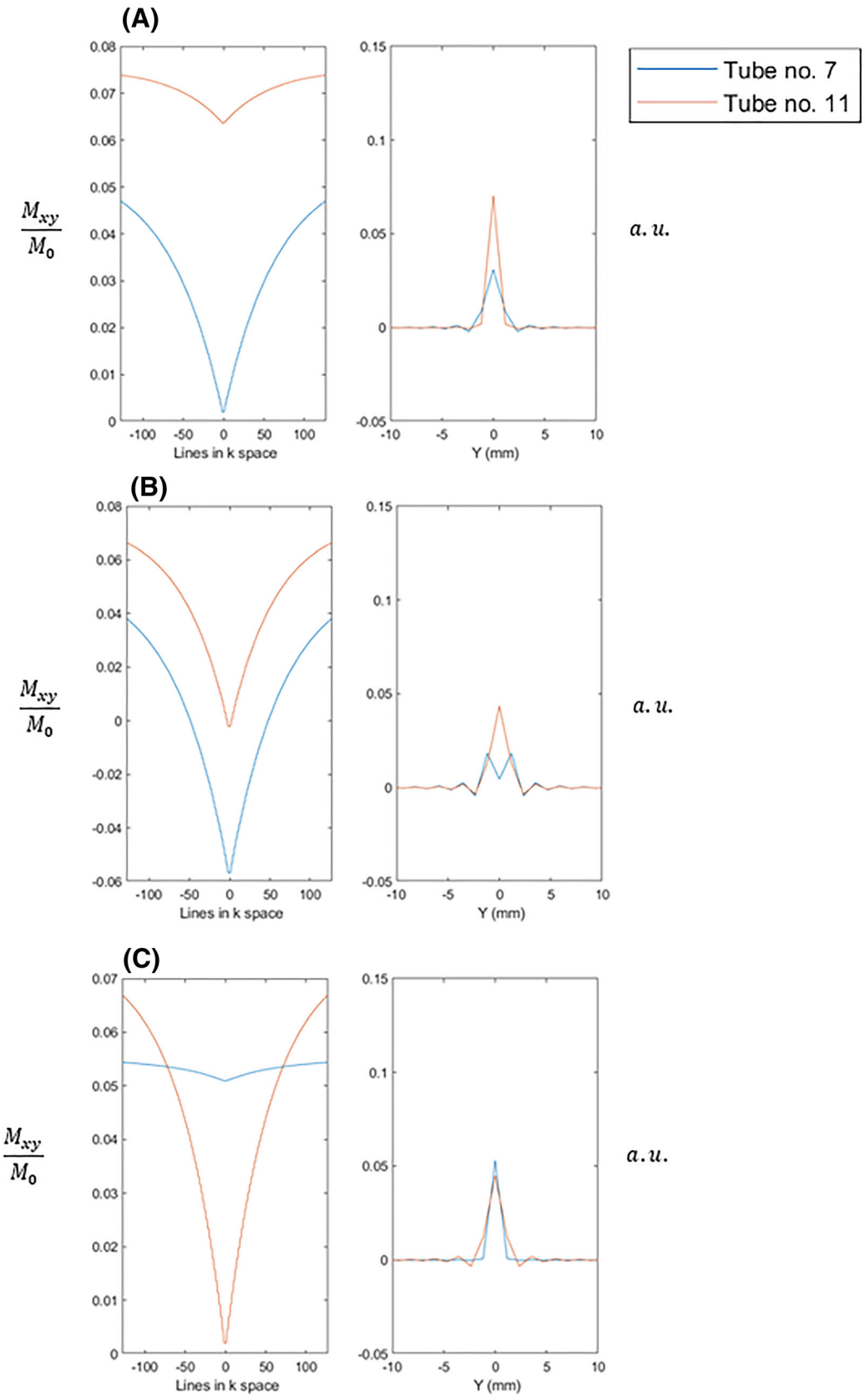

FIGURE 11 Legend on next page.

FIGURE 11 (Left) Normalized signal intensity in the k-space along the k_y direction. (Right) Profile intensity of the point spread function (PSF) calculated in the image space. Red curves correspond to the signal of tube no. 11. Blue curves correspond to the signal of tube no. 7. (A) Two-pulse preparation aiming at maximizing tube no. 11 and saturating tube no. 7. (B) Two-pulse preparation aiming at maximizing tube no. 7 and minimizing tube no. 11. (C) Three-pulse preparation aiming at maximizing tube no. 7 and minimizing tube no. 11 with a cost function that brings the longitudinal magnetization to be maximized (7) to a positive value. In practice for this latter case, preparation is similar to (B), with an additional inversion just before the acquisition. The matrix size is 256 × 256, and the pixel spacing is 1.172 mm.

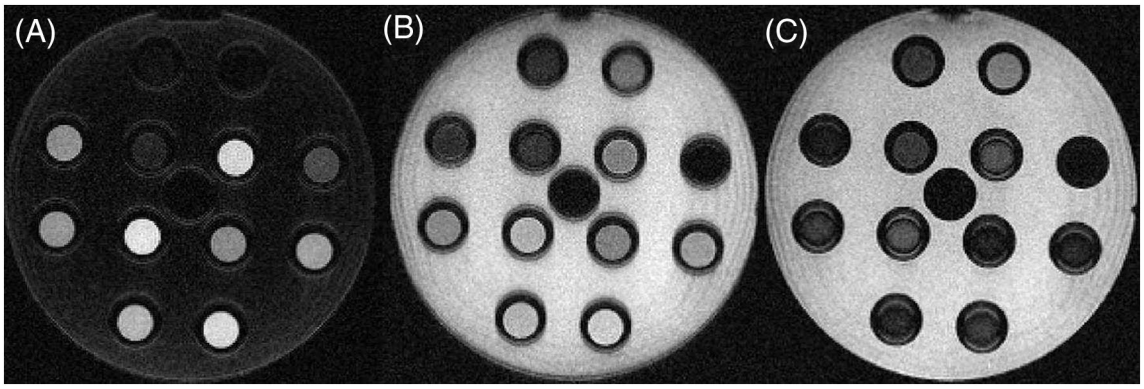

FIGURE 12 Acquisitions corresponding to the signal simulated in Figure 11. (A) Two-pulse preparation aiming at maximizing tube no. 11 and saturating tube no. 7. (B) Two-pulse preparation aiming at maximizing tube no. 7 and minimizing tube no. 11. (C) Three-pulse preparation aiming at maximizing tube no. 7 and minimizing tube no. 11 with a cost function that brings the longitudinal magnetization to be maximized (7) to a positive value. In practice for this latter case, preparation is similar to (B), with an additional inversion just before the acquisition. The matrix size is 256 × 256, and the pixel spacing is 1.172 mm.

TABLE 8 Optimized parameters for contrast problems consisting of saturating one tube (Min) and maximizing another tube (Max) in the case of a 1p-preparation and a 2p-preparation.

Tube Max/Min, N pulses	Preparation module	Signal at first echo (10^{-2})	Time (s)
Contrast between tubes no. 7 and no. 12			
9/12, 1 pulse	$712ms - 180^{\circ}_{x} - 404ms - acq.$	$S_7 = +4.0 \mid S_{12} = +0.1$	22.1
9/12, 2 pulses	$773ms - 92^{\circ}_{x} - 13ms - 88^{\circ}_{x} - 330ms - acq. -$	$S_7 = +4.1 \mid S_{12} = +0.1$	59.7
12/9, 1 pulse	$817ms - 180^{\circ}_{x} - 299ms - acq.$	$S_7 = -0.1 \mid S_{12} = -3.3$	24.4
12/9, 2 pulses	$876ms - 92^{\circ}_{x} - 11ms - 87^{\circ}_{x} - 230ms - acq.$	$S_7 = -0.1 \mid S_{12} = -3.3$	70.8
Contrast between tubes no. 7 and no. 11			
7/11, 1 pulse	$713ms - 180^{\circ}_{x} - 403ms - acq.$	$S_7 = +3.9 \mid S_{11} = +0.0$	22.3
7/11, 2 pulses	$813ms - 91^{\circ}_{x} - 41ms - 86^{\circ}_{x} - 262ms - acq. -$	$S_7 = +5.5 \mid S_{11} = +0.0$	46.1
11/7, 1 pulse	$817ms - 180^{\circ}_{x} - 299ms - acq.$	$S_7 = -0.1 \mid S_{11} = -3.3$	17.0
11/7, 2 pulses	$971ms - 91^{\circ}_{x} - 40ms - 87^{\circ}_{x} - 106ms - acq.$	$S_7 = -0.1 \mid S_{11} = -5.0$	60.8
Contrast between tubes no. 11 and no. 9			
7/12, 1 pulse	$713ms - 180^{\circ}_{x} - 403ms - acq.$	$S_9 = +1.4 \mid S_{11} = +0.1$	27.7
7/12, 2 pulses	$833ms - 91^{\circ}_{x} - 52ms - 86^{\circ}_{x} - 232ms - acq. -$	$S_9 = +1.9 \mid S_{11} = +0.1$	76.1
12/7, 1 pulse	$757ms - 180^{\circ}_{x} - 359ms - acq.$	$S_9 = -0.1 \mid S_{11} = -1.3$	32.2
12/7, 2 pulses	$895ms - 91^{\circ}_{x} - 51ms - 86^{\circ}_{x} - 170ms - acq.$	$S_9 = -0.1 \mid S_{11} = -1.8$	105.8

Mixed T_1 and T_2 weightings in an MP-RAGE sequence are innovative and effective solutions proposed by our algorithm when tissues share similar T_1 but different T_2. Such specific cases can be found in human beings and could suggest potential applications of OC MP-RAGE. In coronary MRI, the oxygenated blood and the deoxygenated blood, as well as the infarcted myocardium and the ventricular blood, share similar T_1, but different T_2. T_2Prep[21] and $T_2Prep - IR$,[23] respectively, have already been developed to address the problem of contrasting these tissues. In the brain region, the WM and the globus pallidus (GP) have a similar T_1[26] but a different T_2 (shorter for the GP around 60 ms[27]). As a result, 2p.-

OCPrep optimized in order to saturate the signal of the WM and to enhance the signal of the GM, also enhances the GP, which is not possible with inversion recovery preparation (Figure 9C,D). Enhancing the contrast between deep brain structures is necessary in the context of DBS for the localization of electrodes. The standard protocol for the localization of the electrodes is composed of T_2-weighted fast spins echo[28] and pure T_1-weighted FGATIR,[7] FLAWS,[26] or MP2RAGE.[29] FGATIR that nulls the WM with an inversion recovery leads to an important loss of signal for the GP, which could be avoided by an optimized 2p.-OCPrep. Future work will investigate the contrast enhancement between deep brain structures where T_2 differences are more important and compared with the standard protocol. As an illustration, acquisitions of the DBS standard protocol have been acquired and are displayed in Figure 9: a standard T_1-weighted MP-RAGE (E), an IR MP-RAGE similar to a FGATIR (C), and a T_2-weighted FLAIR (F).

Some applications require the contrast of more than two tissues. In this context, in neuroimaging, DIR preparation has been used to saturate two tissues of different T_1, usually the CSF and the WM, and was found useful, for example, for the detection of multiple sclerosis lesions.[30] It is usually used inside a spin echo sequence[31] and is optimized by tuning TI_1, TI_2, T_E, and T_R.[32] In the present work, 3p.-OCPrep was optimized to saturate the CSF and WM using both T_1 and T_2 decays. To compare the contrasts achieved with 3p.-OCPrep and standard DIR, a DIR turbo spin-echo (TSE) was acquired on the same volunteer (Figure 10). The inversion times used—$T_{I_1} = 3400$ ms and $T_{I_2} = 325$ ms—were taken from the literature.[31] The effective echo time was 198 ms. Subjective comparison shows better saturation of the WM's signal in the DIR TSE, especially in the frontal area. On the contrary, OC MP-RAGE tends to saturate more of the occipital WM than the frontal WM. From the article by Lu et al.,[33] the values of T_1 and T_2 of the WM are higher in the occipital WM than in the frontal WM (8% and 17%, respectively). In the DIR acquisition, the spin echo acquisitions tend to reinforce the saturation of frontal WM, which has a shorter T_2. Conversely, the structure of 3p.-OCPrep tends more to enhance short T_2 components of the WM and appears to emphasize more the T_2 variations inside the WM. This is particularly visible around the deep brain structures, where the bundles of axons are highlighted (see Figure 9B). In addition, the 3p.-OCPrep MP-RAGE acquisition creates a dark outline between the WM and the GM. This may be due to intravoxel cancelation of the signal of the WM and the GM that have

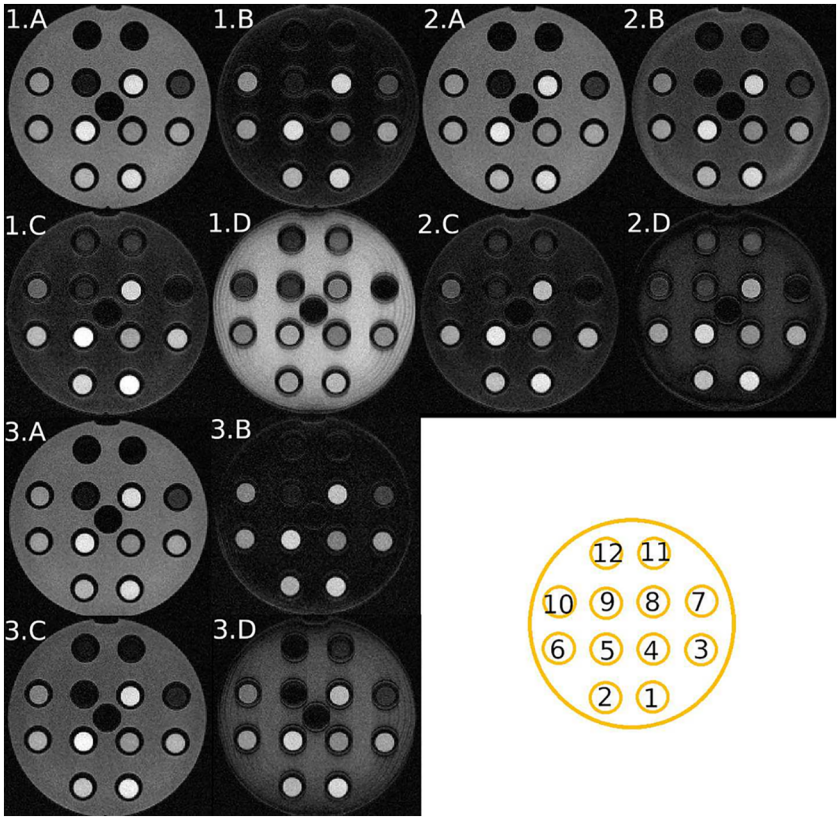

FIGURE 13 MP-RAGE acquisitions with the optimal preparations focusing on the contrast between tubes no. 11 and no. 7 (1), tubes no. 12 and no. 7 (2), and between tubes no. 11 and no. 9 (3). The corresponding numbers of the tubes are indicated in the bottom right hand-right corner. For each case (1, 2, 3, and 4), acquisitions A and B tend to enhance the signal of the tube with the shortest T_1 and T_2 while saturating the signal of the second tube, with, respectively, a 1p.-preparation and 2p.-preparation. For each case (1, 2, 3, and 4), acquisitions and B and C tend to enhance the signal of the tube with the longest T_1 and T_2 while saturating the signal of the second tube, with, respectively, a 1p.-preparation and 2p.-preparation. To compare the advantage of a 2p.-preparation with that of a 1p.-preparation, the same window level is applied for A and B, as well as C and D. MP-RAGE, magnetization-prepared rapid gradient-echo.

opposite phases. Indeed, the polarity of the longitudinal magnetization of the WM and the GM are not the same before being flipped to the transverse plane. This has been described as edge contouring.[34]

Nulling the signal of one or two tissues tends to generate acquisitions with poor SNR. Also, because of the nature of the sequence composed of a rapid spoiled gradient echo, it is easier to enhance the signal of tissues of short T_1 and/or relatively short T_2 (the echo time is 3.2 ms) with an inversion recovery or 2p.-OCPrep.

The spatial resolution of the resulting images was of varying quality according to the cases. For in vivo acquisitions, the resolution in the slab direction is poor due to a limited number of partition encoding steps. To increase the number of partition encodings while keeping the same acquisition duration, a parallel imaging factor could be applied or the number of phase encodings per cycle could be increased. For some in vitro acquisitions, the resolution in the phase direction is poor due to the rapid evolution of the signal during the acquisitions train. It is possible to

TABLE 9 Optimized parameters for contrast problems consisting of saturating one tube and maximizing another tube of shorter T_1 and T_2, in the case of a 1p.-preparation and a 2p.-preparation, for different segment durations ($T_S = 2$, 1.5, 1.25, 1, and 0.75 s).

Segment duration	Preparation module	Signal at first echo (10^{-3})	Time (s)
Contrast between tubes no. 7 and no. 12			
1 pulse			
1500 ms	$712ms - 180^{\circ}_{x} - 404ms - acq.$	$S_7 = +4.0 \mid S_{12} = +0.1$	20.6
1250 ms	$506ms - 180^{\circ}_{x} - 360ms - acq.$	$S_7 = +3.2 \mid S_{12} = +0.1$	20.1
1000 ms	$312ms - 180^{\circ}_{x} - 303ms - acq.$	$S_7 = +2.4 \mid S_{12} = +0.1$	14.5
750 ms	$135ms - 180^{\circ}_{x} - 231ms - acq.$	$S_7 = +1.5 \mid S_{12} = +0.1$	24.5
2 pulses			
1500 ms	$773ms - 92^{\circ}_{x} - 13ms - 88^{\circ}_{x} - 330ms - acq.$	$S_7 = +4.1 \mid S_{12} = +0.1$	58.1
1250 ms	$578ms - 92^{\circ}_{x} - 19ms - 87^{\circ}_{x} - 270ms - acq.$	$S_7 = +3.5 \mid S_{12} = +0.1$	60.2
1000 ms	$382ms - 92^{\circ}_{x} - 24ms - 87^{\circ}_{x} - 208ms - acq.$	$S_7 = +2.8 \mid S_{12} = +0.1$	49.8
750 ms	$193ms - 91^{\circ}_{x} - 29ms - 86^{\circ}_{x} - 143ms - acq.$	$S_7 = +2.0 \mid S_{12} = +0.1$	40.6
Contrast between tubes no. 7 and no. 11			
1 pulse			
1500 ms	$713ms - 180^{\circ}_{x} - 404ms - acq.$	$S_7 = +3.9 \mid S_{12} = +0.1$	38.1
1250 ms	$506ms - 180^{\circ}_{x} - 360ms - acq.$	$S_7 = +3.2 \mid S_{12} = +0.1$	19.1
1000 ms	$313ms - 180^{\circ}_{x} - 303ms - acq.$	$S_7 = +2.4 \mid S_{12} = +0.1$	22.5
750 ms	$135ms - 180^{\circ}_{x} - 231ms - acq.$	$S_7 = +1.5 \mid S_{12} = +0.1$	11.5
2 pulses			
1500 ms	$813ms - 90^{\circ}_{x} - 41ms - 86^{\circ}_{x} - 262ms - acq.$	$S_7 = +5,5 \mid S_{11} = +0.1$	39.5
1250 ms	$595ms - 90^{\circ}_{x} - 42ms - 86^{\circ}_{x} - 227ms - acq.$	$S_7 = +4,9 \mid S_{11} = +0.1$	30.8
1000 ms	$385ms - 90^{\circ}_{x} - 45ms - 84^{\circ}_{x} - 185ms - acq.$	$S_7 = +4.2 \mid S_{11} = +0.1$	50.0
750 ms	$186ms - 87^{\circ}_{x} - 47ms - 81^{\circ}_{x} - 132ms - acq.$	$S_7 = +3.2 \mid S_{11} = +0.1$	27.9
Contrast between tubes no. 9 and no. 11			
1 pulse			
1500 ms	$713ms - 180^{\circ}_{x} - 404ms - acq.$	$S_9 = +1.4 \mid S_{11} = +0.1$	14.4
1250 ms	$506ms - 180^{\circ}_{x} - 360ms - acq.$	$S_9 = +1.1 \mid S_{11} = +0.1$	15.1
1000 ms	$313ms - 180^{\circ}_{x} - 303ms - acq.$	$S_9 = +0.8 \mid S_{11} = +0.1$	15.8
750 ms	$135ms - 180^{\circ}_{x} - 231ms - acq.$	$S_9 = +0.5 \mid S_{11} = +0.1$	17.6
2 pulses			
1500 ms	$813ms - 91^{\circ}_{x} - 52ms - 86^{\circ}_{x} - 232ms - acq.$	$S_9 = +1.9 \mid S_{11} = +0.1$	39.5
1250 ms	$613ms - 91^{\circ}_{x} - 55ms - 86^{\circ}_{x} - 197ms - acq.$	$S_9 = +1.7 \mid S_{11} = +0.1$	30.8
1000 ms	$400ms - 90^{\circ}_{x} - 60ms - 84^{\circ}_{x} - 157ms - acq.$	$S_9 = +1.4 \mid S_{11} = +0.1$	50.0
750 ms	$196ms - 88^{\circ}_{x} - 62ms - 80^{\circ}_{x} - 108ms - acq.$	$S_9 = +1.0 \mid S_{11} = +0.1$	27.9

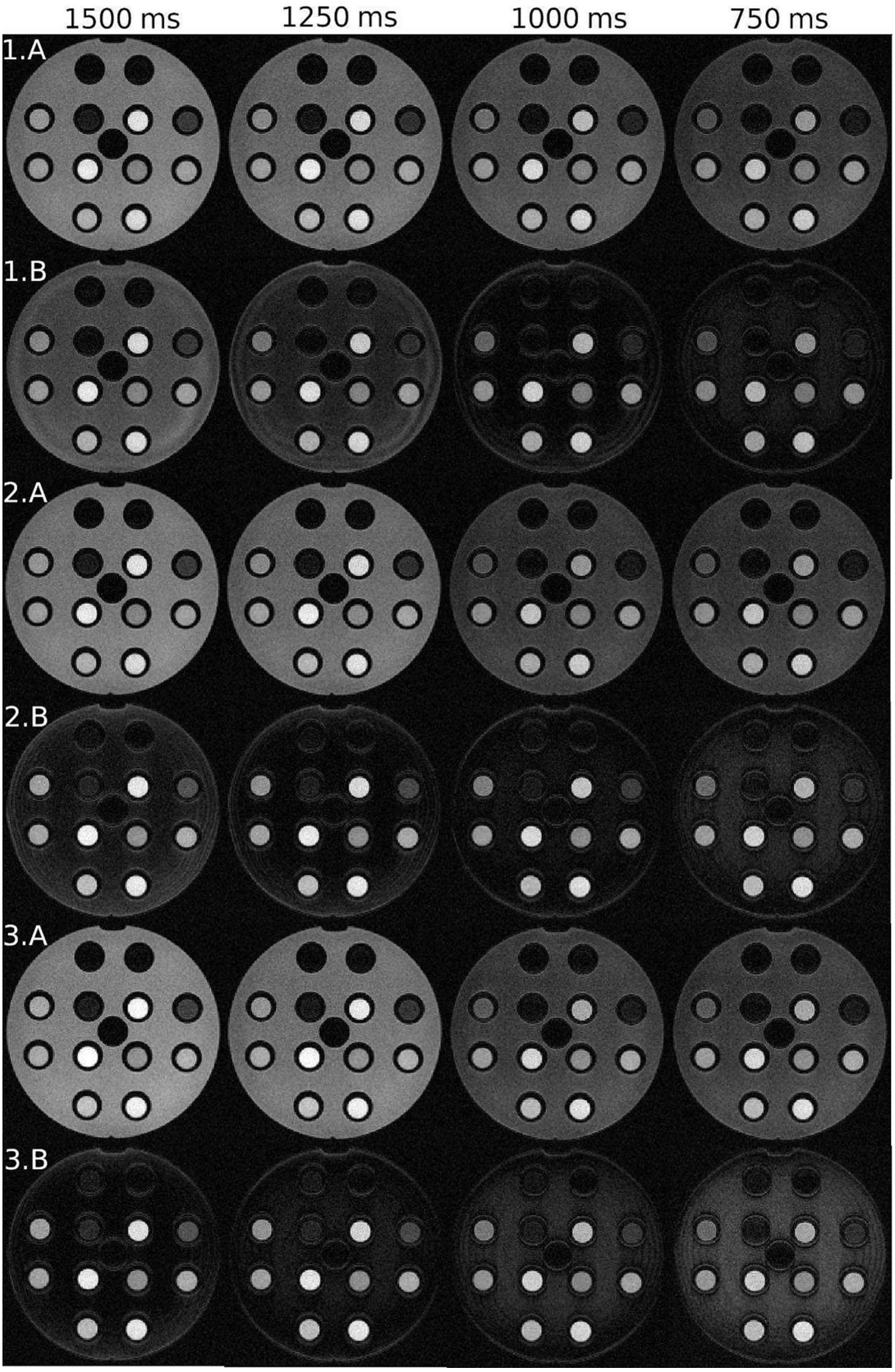

FIGURE 14 Legend on next page.

FIGURE 14 MP-RAGE acquisitions with the optimal preparations focusing on different contrast objectives: (1) saturation of tube no. 12 and enhancement of tube no. 7, (2) saturation of tube no. 11 and enhancement of tube no. 7, and (3) saturation of tube no. 11 and enhancement of tube no. 9. In each case, line A displays the optimal 1p.-preparation for different segment durations from 1500 to 750 ms; line B displays the optimal 2p.-preparation for different segment durations from 1500 to 750 ms. The same window level is applied. MP-RAGE, magnetization-prepared rapid gradient-echo.

anticipate it numerically by computing the point spread function (PSF) of the target tissues in the direction of the phase encoding. For a single value of flip angle α, the evolution of the longitudinal magnetization during the acquisition follows an exponential regrowth from the value at the end of the preparation until the equilibrium value $M_0 S_1 = M_0^*$, as described by Deichmann et al.[8] Rapid variation of the signal can occur when the magnetization at the end of the preparation is far from its equilibrium value, α is high, and/or T_1 is short compared with T_R. It is noticeable that the T_1 values of the used tubes (Spins Safety) are low with respect to in vivo values. This results in a blurring effect that would not happen in vivo. Furthermore, when longitudinal magnetization changes sign during the acquisition, the PSF shape is distorted. In our in vitro results, this happens when seeking to saturate the tissue of the shortest T_1. For example, for the contrast problem between tube no. 7 and no. 11, the numerical PSF is thin when saturating tube no. 11, but widens when saturating tube no. 7 (Figure 11). To correct this problem to some extent, we could have opted for a different cost function, aiming to bring the longitudinal magnetization of the tissue to be maximized to a positive value (without absolute value) as follows:

$$\begin{cases} \min_{\mathbf{u}} C(\mathbf{u}, T_R, \alpha) = -S_{bj} \\ \textit{subject to } S_{aj} = 0. \end{cases} \tag{26}$$

Optimizing a 3p.-preparation to saturate tube no. 7 with this cost function results in a 3.p.-OCPrep scheme, with the final inversion pulses straight before the beginning of the acquisitions train. It improves the numerical computed PSF (Figure 11) and the resolution (Figure 12). However, it limits the space of achievable solutions. Also, to reduce this problem of resolution in the phase direction, we could have modified the acquisition parameters. As described in the method, the flip angle (12°) results from an arbitrary setting up looking for a compromise between the level of signal and the resolution and is quite high compared with standard MP-RAGE protocols. The optimization of variable flip angles jointly to the preparation scheme is currently under investigation and could be presented in future work. Variable flip angles have already been developed in this type of sequence.[35,36] With regard to the T_R, it was set to the minimum possible in the sequence to limit the evolution of the signal from one excitation to the next one. Adding T_R in the optimization problem, that is, differentiating the cost function with respect to the T_R, substantially increases the optimization complexity and usually results in the minimal T_R without introducing significant contrast enhancement.

Moreover, artifacts in the form of concentric rings can be observed in vitro in the case of 2p.-OCPrep or 3p.-OCPrep (see Figures 4D and 5B). They can be attributed to B_0 and B_1 inhomogeneities and pose a challenge in existing 3D T_2*Prep*.[20,37] Indeed, B_1 transmit field of the adiabatic refocusing pulse may be close to the adiabaticity threshold, which leads to a nonuniform cancelation of the effects of B_0 inhomogeneities. As a result of the imperfect magnetization refocusing during the multipulse preparation schemes, some transverse magnetization remains after the 90° storage pulse, leading to undesirable FID signal during the acquisitions. For a short recovery delay separating the preparation pulses from the acquisitions, which is the case in some in vitro experiments, this may lead to the observed ringing artefacts. Artifacts are attenuated for longer delays, as used in vivo. In addition, artifacts can be more visible in vitro, around the interface air/liquid where B_0 inhomogeneities are more important due to the magnetic susceptibility differences.

Eventually, this work, which tends towards determining optimal parameters in a complex steady-state sequence, could be extended to other steady-state sequences, like steady-state free precession sequences. However, the expression of such a steady state would be complex because it requires considering the establishment of the steady state on the three components of the magnetization, whereas the MP-RAGE sequence only requires computation of the equilibrium state along the longitudinal component of the magnetization.

6 | SUPPLEMENTARY MATERIAL

This section presents in detail the numerical results and in vitro results missing in the body of the article.

Table 8 details all the numerical results for the optimal 1p.-preparation and 2p.-preparation modules in order to enhance the contrast between tubes no. 12 and no. 7 (significant differences in T_1 and T_2), no. 11 and no. 7 (large T_2 difference), and eventually tubes no. 9 and no. 11 (small T_1 difference). Figure 13 displays the corresponding acquisitions.

Table 9 details, for the same pairs of tubes, the optimal 1p.-preparation and 2p.-preparation modules in order to enhance the tube of shortest T_2 and T_1 while saturating the other tube for segment durations from 1.5 to 0.75 s (i.e., 1.5, 1.25, 1, and 0.75 s). Figure 14 displays the corresponding acquisitions.

The code has been pushed to a public git repository: https://github.com/vernier-alt/steady_state_article.git.

ACKNOWLEDGMENTS

This work was performed within the framework of the LABEX PRIMES (ANR-11-LABX-0063) of Université de Lyon, within the program "Investissements d'Avenir" (ANR-11-IDEX-0007) operated by the French National Research Agency (ANR). Experiments were carried out with the technical support of the staff of the radiology department at the Centre Léon Bérard. A CC-BY public copyright license has been applied by the authors to the present document and will be applied to all subsequent versions up to the Author Accepted Manuscript arising from this submission, in accordance with the grant's open access conditions.

REFERENCES

1. Mugler JP, Brookeman JR. Three-dimensional magnetization-prepared rapid gradient-echo imaging (3D MP RAGE). *Magn Reson Med*. 1990;15(1):152-157. doi:10.1002/mrm.1910150117
2. Epstein FH, Mugler JP, Brookeman JR. Spoiling of transverse magnetization in gradient-echo (GRE) imaging during the approach to steady state. *Magn Reson Med*. 1996;35(2):237-245. doi:10.1002/mrm.1910350216
3. Mugler JP, Brookeman JR. Rapid three-dimensional T1-weighted MR imaging with the MP-RAGE sequence. *J Magn Reson Imaging*. 1991;1(5):561-567. doi:10.1002/jmri.1880010509
4. Mugler JP, Spraggins TA, Brookeman JR. T2-weighted three-dimensional MP-RAGE MR imaging. *J Magn Reson Imaging*. 1991;1(6):731-737. doi:10.1002/jmri.1880010621
5. Epstein FH, Mugler JP, Cail WS, Brookeman JR. CSF-suppressed T2-weighted three-dimensional MP-RAGE MR imaging. *J Magn Reson Imaging*. 1995;5(4):463-469. doi:10.1002/jmri.1880050417
6. Jack CR, Bernstein MA, Fox NC, et al. The Alzheimer's disease neuroimaging initiative (ADNI): MRI methods. *J Magn Reson Imaging*. 2008;27(4):685-691. doi:10.1002/jmri.21049
7. Sudhyadhom A, Haq IU, Foote KD, Okun MS, Bov FJ. A high resolution and high contrast MRI for differentiation of subcortical Structures for DBS targeting: the fast gray matter acquisition T1 inversion recovery (FGATIR). *Neuroimage*. 2009;47:T44-T52. doi:10.1016/j.neuroimage.2009.04.018
8. Deichmann R, Good CD, Josephs O, Ashburner J, Turner R. Optimization of 3-D MP-RAGE sequences for structural brain imaging. *Neuroimage*. 2000;12(1):112-127. doi:10.1006/nimg.2000.0601
9. Vernier B, Van Reeth E, Pilleul F, Beuf O, Ratiney R. MRI contrast enhancement of magnetization prepared steady state sequence: an optimal control framework. Nice, France: IEEE, April 2021, 1709-1713. 10.1109/ISBI48211.2021.9434151
10. Khaneja N, Reiss T, Kehlet C, Schulte-Herbrüggen T, Glaser SJ. Optimal control of coupled spin dynamics: design of NMR pulse sequences by gradient ascent algorithms. *J Magn Reson*. 2005;172(2):296-305. doi:10.1016/j.jmr.2004.11.004
11. Van Reeth E, Ratiney H, Tse Ve Koon K, et al. A simplified framework to optimize MRI contrast preparation. *Magn Reson Med*. 2019;81(1):424-438. doi:10.1002/mrm.27417
12. Van Reeth E, Ratiney H, Lapert M, Glaser SJ, Sugny D. Optimal control theory for applications in magnetic resonance imaging. *Pac J Math Ind*. 2017;9(1):9. doi:10.1186/s40736-017-0034-3
13. Han SP. A globally convergent method for nonlinear programming. *J Optim Theory Appl*. 1977;22:297-309.
14. Broydon - Fletcher - Goldfarb - Shanno (BFGS) method. Accessed April 14, 2022. https://fr.mathworks.com/matlabcentral/fileexchange/31237-broydon-fletcher-goldfarb-shanno-bfgs-method
15. Norris DG, Böttcher U, Leibfritz D. A simple method of generating variable T1 contrast images using temporally reordered phase encoding. *Magn Reson Med*. 1990;15(3):483-490. doi:10.1002/mrm.1910150315
16. Holsinger AE, Riederer SJ. The importance of phase-encoding order in ultra-short TR snapshot MR imaging. *Magn Reson Med*. 1990;16(3):481-488. doi:10.1002/mrm.1910160315
17. Bojorquez JZ, Bricq S, Acquitter C, Brunotte F, Walker PM, Lalande A. What are normal relaxation times of tissues at 3 T? *Magn Reson Imaging*. 2017;35:69-80. doi:10.1016/j.mri.2016.08.021
18. Spijkerman JM, Petersen ET, Hendrikse J, Luijten P, Zwanenburg JJM. T2 mapping of cerebrospinal fluid: 3 T versus 7 T. *Magn Reson Mater Phys Biol Med*. 2018;31(3):415-424. doi:10.1007/s10334-017-0659-3
19. Boulby PA, Symms MR, Barker GJ. Optimized interleaved whole-brain 3D double inversion recovery (DIR) sequence for imaging the neocortex. *Magn Reson Med*. 2004;51(6):1181-1186. doi:10.1002/mrm.20088
20. Nezafat R, Stuber M, Ouwerkerk R, Gharib AM, Desai MY, Pettigrew RI. B1-insensitiveT2 preparation for improved coronary magnetic resonance angiography at 3 T. *Magn Reson Med*. 2006;55(4):858-864. doi:10.1002/mrm.20835
21. Brittain JH, Hu BS, Wright GA, Meyer CH, Macovski A, Nishimura DG. Coronary angiography with magnetization-prepared T2 contrast. *Magn Reson Med*. 1995;33(5):689-696. doi:10.1002/mrm.1910330515
22. Liu CY, Bley TA, Wieben O, Brittain JH, Reeder SB. Flow-independent T2-prepared inversion recovery black-blood MR imaging. *J Magn Reson Imaging*. 2010;31(1):248-254. doi:10.1002/jmri.21986
23. Liu CY, Wieben O, Brittain JH, Reeder SB. Improved delayed enhanced myocardial imaging with T2-Prep inversion recovery magnetization preparation. *J Magn Reson Imaging*. 2008;28(5):1280-1286. doi:10.1002/jmri.21560
24. Lu H, Clingman C, Golay X, van Zijl PCM. Determining the longitudinal relaxation time (T1) of blood at 3.0 Tesla. *Magn Reson Med*. 2004;52(3):679-682. doi:10.1002/mrm.20178
25. Zhao JM, Clingman CS, Närväinen MJ, Kauppinen RA, van Zijl PCM. Oxygenation and hematocrit dependence of transverse relaxation rates of blood at 3T. *Magn Reson Med*. 2007;58(3):592-597. doi:10.1002/mrm.21342
26. Tanner M, Gambarota G, Kober T, et al. Fluid and white matter suppression with the MP2RAGE sequence. *J Magn Reson Imaging*. 2012;35(5):1063-1070. doi:10.1002/jmri.23532

27. Dezortova M, Lescinskij A, Dusek P, et al. Multiparametric quantitative brain MRI in neurological and hepatic forms of Wilson's disease. *J Magn Reson Imaging*. 2020;51(6):1829-1835. doi:10.1002/jmri.26984
28. Pinsker MO, Volkmann J, Falk D, et al. Deep brain stimulation of the internal globus pallidus in dystonia: target localisation under general anaesthesia. *Acta Neurochir*. 2009;151(7):751-758. doi:10.1007/s00701-009-0375-5
29. Shipp D, Kober T. FLAWS and MP2RAGE sequence at 3T for surgical localization in pre deep brain stimulator patients. *MAGNETOM Flash*. 2017;69(4).
30. Higazi MM, Ghany HSAE, Fathy AW, Ismail MM, Samra MFA. Diagnostic accuracy of double inversion recovery (DIR) in detection of cortical gray matter lesions in patients with MS. *Egypt J Radiol Nucl Med*. 2022;53(1)):13. doi:10.1186/s43055-021-00668-x
31. Wattjes MP, Lutterbey GG, Gieseke J, et al. Double inversion recovery brain imaging at 3T: diagnostic value in the detection of multiple sclerosis lesions. *AJNR Am J Neuroradiol*. 2007;28(1):54-59.
32. Redpath TW. Technical note: use of a double inversion recovery pulse sequence to image selectively grey or white brain matter. *Br J Radiol*. 1994;67(804)):1258-1263. doi:10.1259/0007-1285-67-804-1258
33. Lu H, Nagae-Poetscher LM, Golay X, Lin D, Pomper M, van Zijl PCM. Routine clinical brain MRI sequences for use at 3.0 Tesla. *J Magn Reson Imaging*. 2005;22(1):13-22. doi:10.1002/jmri.20356
34. Middlebrooks EH, Lin C, Westerhold E, et al. Improved detection of focal cortical dysplasia using a novel 3D imaging sequence: edge-enhancing gradient echo (3D-EDGE) MRI. *NeuroImage Clin*. 2020;28:102449. doi:10.1016/j.nicl.2020.102449
35. Epstein FH, Mugler JP, Brookeman JR. Optimization of parameter values for complex pulse sequences by simulated annealing: application to 3D MP-RAGE imaging of the brain. *Magn Reson Med*. 1994;31(2):164-177. doi:10.1002/mrm.1910310210
36. Mugler JP, Epstein FH, Brookeman JR. Shaping the signal response during the approach to steady state in three-dimensional magnetization-prepared Rapid gradient-echo imaging using variable flip angles. *Magn Reson Med*. 1992;28(2)):165-185. doi:10.1002/mrm.1910280202
37. Nezafat R, Ouwerkerk R, Derbyshire AJ, Stuber M, McVeigh ER. Spectrally selective B1-insensitive T2 magnetization preparation sequence. *Magn Reson Med*. 2009;61(6):1326-1335. doi:10.1002/mrm.21742

How to cite this article: Vernier B, Van Reeth E, Pilleul F, Lapert M, Beuf O, Ratiney H. Optimal control in a magnetization-prepared rapid acquisition gradient-echo sequence. *NMR in Biomedicine*. 2023;e5041. doi:10.1002/nbm.5041